REVIEW

Check for updates

Superwetting Janus membranes: focusing on unidirectional transport behaviors and multiple applications

Hui Zhou[ab] and Zhiguang Guo (iD) *[ab]

It should be noted that the one-way transportation of liquids is of great significance to the separation or collection process and the manipulation of microfluids can effectively solve many practical problems, such as oil–water separation, fog-harvesting and so on. Fortunately, asymmetric wettability endows bioinspired Janus membranes (JMs) with special driving forces for unidirectional liquid transportation, which is of great potential in microfluidic manipulation. In this review, recent research advances in JMs are summarized with the focus on the development process, basic wetting properties and classifications of JMs. Based on different prepared materials, bioinspired special JMs can be divided into three categories as follows: polymeric Janus membranes, polymeric-inorganic Janus membranes and inorganic Janus membranes. Next, special attention is paid to the systematic physical mechanisms of unidirectional transport. Also outlined are current and potential applications in oil–water separation, membrane distillation, fog-harvesting, sensors and so on. Finally, a perspective on the future of bioinspired superwetting JM research and development is proposed.

[a]Hubei Collaborative Innovation Centre for Advanced Organic Chemical Materials, Ministry of Education, Key Laboratory for the Green Preparation and Application of Functional Materials, Hubei University, Wuhan 430062, People's Republic of China
[b]State Key Laboratory of Solid Lubrication, Lanzhou Institute of Chemical Physics, Chinese Academy of Sciences, Lanzhou 730000, People's Republic of China. E-mail: zguo@licp.cas.cn; Fax: +86-931-8277088; Tel: +86-931-4968105

1 Introduction

In ancient Roman mythology, Janus is a God who has two faces to better examine the past and future.[1] As is well known, the term "Janus materials" to describe the asymmetric surface wettability of a spherical glass bead was first adopted by C. Casagrande in 1988.[2] Since then, Janus materials have attracted great interest, but they were not widely spread until Pierre-Gilles

Miss Hui Zhou joined Prof. Guo's biomimetic materials of tribology (BMT) group at Hubei University in 2018 to pursue her PhD degree. Her current scientific interests are focused on superwetting Janus membranes with unidirectional transport behaviors and their multiple applications.

Professor Zhiguang GUO received his PhD from Lanzhou Institute of Chemical Physics (LICP), Chinese Academy of Sciences (CAS) in 2007. After that, he joined Hubei University. From Oct 2007 to Aug 2008, he worked at University of Namur (FUNDP), Belgium, as a post-doc. From Sep 2008 to Mar 2011, he worked in Funds of National Research Science (FNRS), Belgium, as a "Charge de Researcher". During Feb 2009 to Feb 2010, he worked in the Department of Physics, University of Oxford, UK, as a visiting scholar. Now he is a full professor in LICP financed by the "Top Hundred Talents" program of CAS. Until now, he has published more than 250 papers about the interfaces of Materials.

This journal is © The Royal Society of Chemistry 2019

J. Mater. Chem. A, 2019, 7, 12921–12950 | 12921

de Gennes gave his Nobel lecture in 1991.[3] Janus materials with entirely different properties or components on two faces have received great attention from various research fields for applications, such as oil–water separation,[4,5] sensors,[6] fog harvesting,[7] and so on. The unusual Janus materials show big advantages when compared with homogeneous materials due to their high selectivity.[8,9]

Since the concept of Janus materials was invented, the main research has focused on the preparation, characterization and applications of Janus particles,[10] such as micelles,[11] sheets[12] and rods.[13] Meanwhile, research on Janus membranes, a kind of Janus derived material, has also been developed in recent years, which resulted in the emergence of different types of Janus membranes (JMs), including hybrid MWCNT membranes with well-tunable wettability,[14] electrospun nanofiber Janus membranes[15] and thin porous Janus membranes.[16]

Janus interface materials refer to two-dimensional and three-dimensional porous materials with asymmetric properties on each face, resulting from different structures and components.[17–19] Furthermore, materials with similar properties exist widely in nature and they are crucial for living organisms. For instance, the lotus leaf structure is a typical example of a Janus interface: its upper side is superhydrophobic (solid surfaces with a static water contact angle $\theta > 150°$ and a sliding angle less than 10°), while the lower side is hydrophilic and underwater super-oleophobic (in the oil/water/solid system, solid surfaces with a static oil contact angle larger than 150° and a sliding angle less than 10°), as illustrated in Fig. 2a.[20,21] It is worth noting that solid surfaces with a water contact angle $\theta > 90°$ are defined as hydrophobic according to Young's equation. However, using a surface force apparatus supported by ancillary techniques, Vogler demonstrated that a CA of 65° divides solid materials into hydrophobic and hydrophilic, rather than 90° as in the mathematical concept.[22] According to the summary of papers on JMs published in recent years, researchers have shown great interest since the concept of Janus membranes was proposed, and research on JMs has been increasing year by year, denoting their rapid development in the latest decade (see Fig. 1). To date, it should be noted that there are many different configurations of JMs.[23] To better exhibit the configurations of JMs, JMs can be

divided into two interconnected regions, the upper layer and the lower layer. In addition, according to the thickness of each layer, JMs have three typical constituent modes, including different thicknesses of the upper and lower layers, similar thicknesses of the upper and lower layers, and a fusion of the upper and lower layers. According to different experimental purposes, methods for preparing JMs are also different. In previous studies, many methods for preparing JMs have appeared, including sequential electrospinning,[24,25] vacuum filtration,[26] one-side electro-spraying,[27] etc.[28–31] Based on the analysis of the prepared materials, JMs can be divided into three categories, including polymeric Janus membranes, polymeric-inorganic Janus membranes and inorganic Janus membranes. Generally, obtaining JMs by asymmetric fabrication is a simple way. Furthermore, this method involves the fabrication of each side of JMs respectively followed by combining them together. In addition, JMs can also be obtained by asymmetric decoration, which is single-face modification with different materials.

In addition, with the development of surface science, surfaces with special wettability, such as gradient or reversible, gradually become the focus of the field now.[32,33] It was found that JMs consisting of two closely contacted layers with opposite wettability have such special properties. Researchers have fabricated similar structures in artificial membranes inspired by the heterogeneous structures of aquaporin, which can facilitate water transport across the cell membrane.[34] Influenced by such a phenomenon, previous research concerning common materials and JMs mainly concentrated on unidirectional liquid transport.[35–38] Take lyophilic/lyophobic (solid surfaces with a liquid contact angle $\theta > 90°$ and $\theta < 90°$) Janus membranes as an example, the liquid droplet gradually penetrates into the membrane from the lyophobic layer, but cannot transfer from the lyophilic layer to the lyophobic layer (see Fig. 2c).[39] Asymmetric wettability endows bioinspired JMs with special driving forces for unidirectional liquid transport, distinguishing them from normal membranes with homogeneous wettability. Furthermore, unidirectional liquid transport can also happen against gravity without any external force.[40] Recently, Janus materials such as Janus meshes and JMs with unidirectional transport properties of gas bubbles have also been reported,[41,42] where gas bubbles can penetrate through the thickness of the materials from one side to another, while their transport is blocked in the reverse direction (see Fig. 2b). The unidirectional transport behaviors of liquids and gas bubbles in some JMs are also referred to as "one-way" transport. Generally, these behaviors can be driven by various forces, such as the Laplace pressure, gravity and external force.[43,44] Owing to the asymmetric wettability of JMs, the Laplace pressure will be generated, promoting the occurrence of unidirectional transport behaviors even without extra energy. A comparison of JMs with normal membranes which have homogeneous wettability shows that the typical difference is the anisotropic breakthrough pressure in the cross-section direction.[45] There is no doubt that these special features provide JMs with enormous potential in microfluidic manipulation and novel applications.

In early reviews, Pang et al.[46] and Hu et al.[12] summarized the preparation of chemical or morphological gradients on Janus
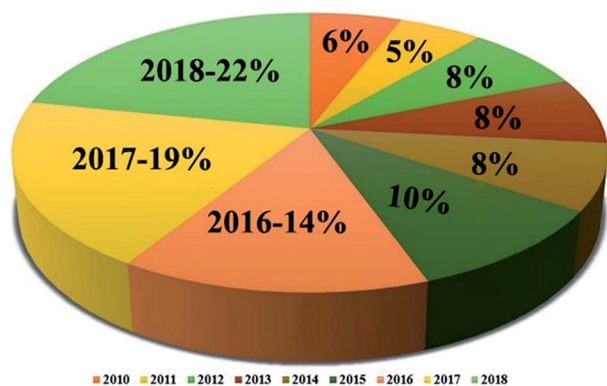

Fig. 1 The percentages of published papers on Janus membranes retrieved from Web of Science in the latest decade.

12922 | J. Mater. Chem. A, 2019, 7, 12921–12950

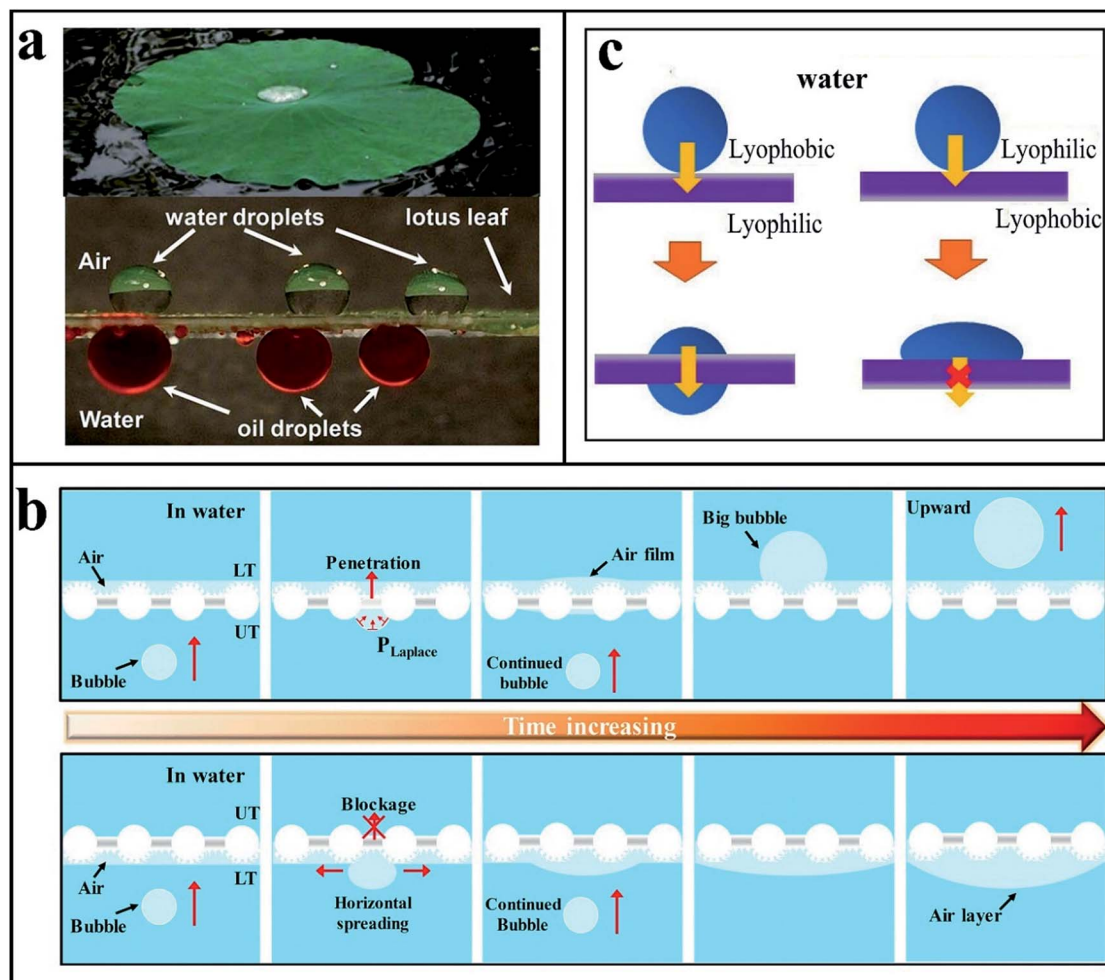This journal is © The Royal Society of Chemistry 2019

Fig. 2 (a) Digital photographs of a lotus leaf floating on the water surface showing different wettabilities for water and oil droplets. Reproduced with permission.[20] Copyright 2011, Royal Society of Chemistry. (b) Schematic of the mechanism of the asymmetrical PTFE mesh for the unidirectional transportation of gas bubbles. Adapted with permission.[41] Copyright 2018, American Institute of Physics. (c) One-way water-transport effect: When the water droplet is dripped on the lyophobic side, it will permeate through the lyophobic layer to the lyophilic layer. In the opposite direction, it is blocked and no penetration occurs. Reproduced with permission.[39] Copyright 2016, Wiley-VCH.

particles. However, research about the preparation and unidirectional transport behaviors of fluid and gas bubbles on JMs has been rarely reviewed so far. In this review, recent research advances in JMs are summarized with the focus on the development process, basic wetting properties and classifications of JMs. After introducing recent advances in synthetic methodology, the phenomena of the unidirectional transport behaviors of fluid and gas bubbles and systematic physical mechanisms are explained and discussed, respectively. Next, several representative performances and current applications of JMs will be discussed in more detail. Owing to their limitations and potential applications, research on JMs, ranging from their facile fabrication to novel applications, is necessary.

2 Design principles and classifications

2.1 Structures of Janus membranes and fundamental design principles

It is well known that the Janus membrane has asymmetric wettability characteristics. JMs consist of two interconnected regions, where the wettability is completely different as well as the wettability of each layer is homogeneous. Whether the Janus membrane is a bilayered or trilayered structure, the wettability gradient tends to change gradually along the cross-section direction of the membrane. To better exhibit the structures of JMs, we divide the two interconnected regions into the upper layer and the lower layer. In addition, according to the thickness of each layer, JMs have many constituent modes, including different thicknesses of the upper and lower layers, similar thicknesses of the upper and lower layers, and a fusion of the upper and lower layers. Before preparing JMs, it is necessary to consider the total thickness of JMs and the thickness distribution of each layer. Based on this factor, different thickness distributions of each layer determine different applications of JMs. For the thickness of the lyophobic layer, the penetration of liquids can be divided into three categories. When the lyophobic layer is too thin, the resistance to the liquid is greatly reduced, causing the liquid to penetrate through the Janus membrane from either side. When the thickness of the

lyophobic layer is appropriate, the liquid can penetrate from the lyophobic side to the lyophilic side, whereas it cannot penetrate through the membrane in the opposite direction. As for the unidirectional transport behavior of droplets on a Janus membrane, there is a resistance for droplet on the lyophobic layer and an attraction on the lyophilic layer. When the lyophobic layer is too thick, the resistance is far greater than attraction and the droplets cannot penetrate through it to the lyophilic layer, leading to that the Janus membrane becomes a material that is impermeable to the liquid. Similarly, for the thickness analysis of the underwater aerophobic (a contact angle greater than 90° to a small bubble in water) layer of a Janus membrane, the directional transport behavior of gas bubbles is similar to that of the liquid on the lyophobic layer.

In recent years, a large number of studies on JMs have appeared in various preparation rules. Here, the design of JMs can be discussed from two aspects, including factors affecting the extreme wettability of the membrane surface and classifications of preparation methods of JMs based on the macroscopic perspective.

To the best of our knowledge, surface wettability is mainly governed by both the surface chemistry and surface microstructure.[47,48] It has been found that a single micro- or nanoscale rough surface can increase the wettability of the original substrate surface, either hydrophobic or hydrophilic and the micro/nanoscale hierarchical structure can further lead to a greater enhancement of wettability than the former.[49]

Surface roughness can be designed to capture or repel a significant amount of air pockets inside gaps in the microstructure, creating superlyophobic or superlyophilic surfaces that can repel or attract various types of liquids respectively and the specific theoretical analysis is in Section 3.1. Next, several extreme wettability surfaces will be taken as examples. For the superhydrophobic layer, the design principle derived from natural examples is that the chemical composition of the membrane surface should be hydrophobic. Apart from the chemical composition, the surface structure plays a vital role in surface wettability. Therefore, the rule for constructing superhydrophobic surfaces is to introduce sufficient surface roughness on the natural hydrophobic surface. Similarly, the principle of construction of superhydrophilic (solid surfaces with a static water contact angle close to 0°) surfaces can also be divided into two types, generating sufficient roughness on the membrane surfaces and tailoring the chemical compositions of membrane surfaces to be hydrophilic. In order to prepare a superoleophobic (solid surfaces with a static oil water contact angle $\theta > 150°$, a sliding angle less than 10°, the contact angle hysteresis $\Delta\theta < 5°$ and the tilt angle less than 5°) surface, it is necessary to consider the attractive forces between the oil molecules and the solid surface molecules, which may support the oil to wet the surface. Specifically, repellency of various low adhesion organic liquids can be achieved by introducing sufficient roughness while incorporating the construction of a low surface energy fluorinated layer.

Moreover, it is worth noting that a type of Janus membrane has asymmetric wettability, providing it with unidirectional transport performance. On one surface, its wetting is

hydrophobic or superhydrophobic while the wetting on the other surface is exactly the opposite. In addition, owing to the gradient of the surface energy or roughness, the self-driving force can be generated from the two sides of Janus membranes. On the basis of these unique properties and preparation processes, the design strategy of JMs can be divided into two categories. The first type of preparation method is that fabricating each layer of the Janus membrane respectively and then combining them together. Another popular method is to modify the membrane and the specific preparation method is given in Section 2.2. In either of the two design strategies, the desired wettability can be achieved by carefully selecting surface chemical compositions, designing microstructures or regulating surface roughness on both sides of the JMs.

2.2 Classifications of Janus membranes

In recent years, there are more and more specific methods for preparing JMs, including sequential electrospinning,[24,25,50] one-side electrospraying,[27,51] *etc.*[52–57] By analysing and summarizing the prepared materials, JMs can be divided into four categories: polymeric Janus membranes, polymeric-inorganic Janus membranes, inorganic Janus membranes and other Janus membranes (see Fig. 3). Generally speaking, the first type of JMs can be obtained by asymmetric fabrication, where each side of JMs may need to be fabricated by using polymers of different properties respectively followed by combining them together. The second type of JMs can be made by modifying a polymer onto an inorganic (metal or non-metal) substrate. Besides, there are lots of emerging methods for efficient and rapid preparation, including one-step laser-processing of superhydrophobic patterns on pristine hydrophilic copper sheets[58] and using technologies to change the structure on one side of the Janus membrane.[59] Table 1 summarizes representative studies on JMs, which include prepared materials, preparation methods, design principles, wettability and applications of each study.

2.2.1 Polymeric Janus membranes. Polymeric Janus membranes have attracted tremendous interest from fundamental research to both industrial and academic areas because of their potential applications.[60,61] Many efficient methods have been reported towards the fabrication of polymeric Janus membranes, typically including sequential electrospinning and sequential vacuum filtration. It should be noted that it is efficient to obtain different JMs through fabricating each layer of the membrane respectively and then combining them together. When using two polymers to fabricate Janus structures, two different functions can be obtained through two polymers.

The most prevalent method for fabricating polymeric Janus membranes is sequential electrospinning. For the electrospun Janus membrane, it is easy to prepare and the thickness of each side can be adjusted through electrospinning time.

Take an electrospun oleophobic/oleophilic (solid surface with a static oil contact angle $\theta < 90°$) Janus membrane as an example,[62] it was prepared by a layered electrospinning technique using PVDF-HFP and PVDF-HFP containing well-dispersed FD-POSS and FAS as materials (shown in Fig. 4a and b). The prepared Janus membrane had different wettability
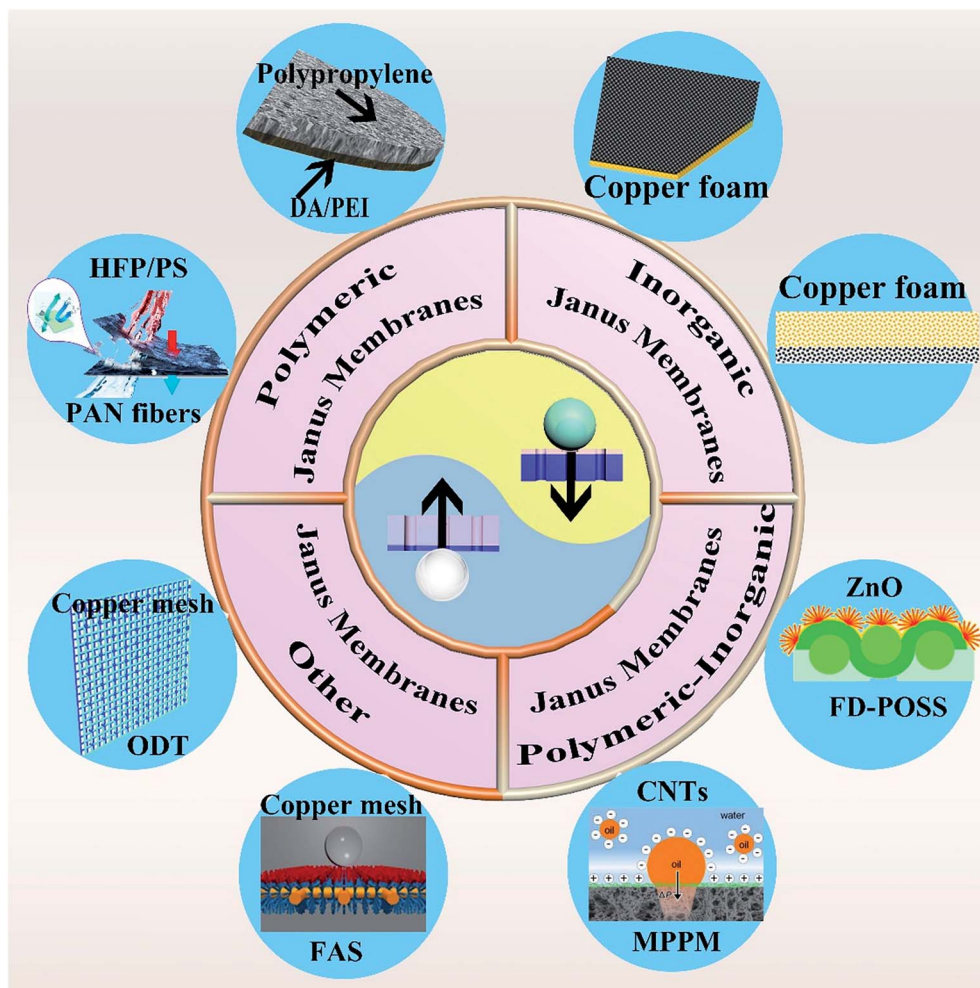
12924 | *J. Mater. Chem. A*, 2019, **7**, 12921–12950

This journal is © The Royal Society of Chemistry 2019

Fig. 3 Schematic diagram of classifications of Janus membranes. Typical Janus membranes: polymeric JMs, (Reproduced with permission.[51] Copyright 2018, Elsevier B. V. Reproduced with permission.[56] Copyright 2016, Wiley-VCH), polymeric–inorganic JMs, (Reproduced with permission.[63] Copyright 2015, American Chemical Society. Reproduced with permission.[128] Copyright 2018, American Chemical Society.), inorganic JMs, (Reproduced with permission.[58] Copyright 2018, American Chemical Society. Reproduced with permission.[64] Copyright 2018, American Institute of Physics), and other JMs (Reproduced with permission.[53] Copyright 2017, Wiley-VCH. Reproduced with permission.[123] Copyright 2019, Royal Society of Chemistry).

on both layers, being superhydrophobic and oleophilic on the PVDF-HFP layer while superamphiphobic on the PVDF-HFP/FD-POSS/FAS layer.

With the rapid growth of economy, it is significant to prepare polymeric Janus membranes on a large scale. A distinctive type of Janus ultrafine fibre membrane (UFM) *via* electrospinning by Geng *et al.*[50] was successfully fabricated on a large scale. In their work, they chose two types of polymers, polyacrylonitrile (PAN) and polyvinylpyrrolidone (PVP), to fabricate JMs. Interestingly, it would be better if both spinning polymers can be dissolved in the same solvent. PVP and PAN were used in electrospinning and both were dissolved in *N,N*-dimethylformamide (DMF), and the UFMs were collected on aluminum foil at high voltage.

In addition, traditional methods such as polymerization deposition and spray coating are not feasible for conventional membranes due to their uncontrollable operation and extensive membrane pore blocking. Nevertheless, the combination of

different preparation methods, such as electrospinning and electrospray, not only improves the performance of Janus membranes, but also controls the operation steps with high efficiency. For example, Zhu *et al.*[51] reported an asymmetrically superwettable Janus membrane which was developed *via* sequential electrospinning and electrospraying. It was found that the asymmetrically superwettable Janus membrane had an electrospun hydrophobic PVDF nanofibrous membrane (NFM) to prevent membrane fouling and keep membrane durability. As shown in Fig. 4c. PVDF membrane substrates were fabricated *via* electrospinning of a LiCl/PVDF solution. Then, F-SiO$_2$@-PVDF-HFP/PS and SiO$_2$@PAN solution were used to prepare the Janus skin layer with asymmetric superwettability *via* a sequential electrospraying technique.

Besides the methods mentioned above, Yang and co-workers[56] reported a Janus membrane obtained by floating an ethanol prewetted polypropylene membrane on a DA/PEI

This journal is © The Royal Society of Chemistry 2019

J. Mater. Chem. A, 2019, **7**, 12921–12950 | **12925**

Table 1 Classifications of Janus membranes, including prepared materials, preparation methods, design principles, wettability and applications

	Materials	Preparation	Design principle	Wettability	Major applications	Ref.
Polymeric JMs	Polyacrylate PSA (HPSA) and c-PVA	Sequential electrospinning	Double-layer composite	Hydrophobic/ hydrophilic	Transdermal drug delivery system	24
	PVDF-HFP and PVDF-HFP/FD-POSS/FAS	Sequential electrospinning	Double-layer composite	Superhydrophobic–oleophilic/ superamphiphobic	Oil–water separation	62
	PVP and PAN	Sequential electrospinning	Double-layer composite	Hydrophilic/ hydrophobic	Biphasic drug release	50
	PS/PVDF-HFP and PAN	Sequential electrospinning and electrospraying	Double-layer composite	Superhydrophobic/ superhydrop-hilic	Membrane distillation	51
	Polypropylene membrane and PDA/PEI	Single-side deposition	Single-layer modification	Hydrophilic–superareophobic/ hydrophobic–aerophilic	Fine bubble aeration	56
	PDMAEMA/PDMS	Grafting method	Single-layer modification	Superhydrophobic/ superhydrophilic	Oil–water separation	127
Polymeric-inorganic JMs	ZnO and FD-POSS/FAS	A two-step coating technique and subsequent UV treatment	Single-layer modification	Hydrophilic/ superhydrophobic	Gauging liquid surface tension	63
	ZnO-Kevlar pieces and FeOOH-Kevlar pieces	Vacuum filtration	Double-layer composite	Superhydrophobic/ hydrophilic	Separating diffident types of emulsions	52
	Graphene oxide/chitosan hybrid membrane, PS and PDMAEMA	Photo-grafting and photo-polymerization	Single-layer modification	Hydrophobic/ hydrophilic	—	57
	Copper mesh and PTFE	Femtosecond laser treated	Single-layer modification	Hydrophilic/ superhydrophobic	Fog collection	121
	Copper mesh, cotton absorbent	—	—	Hydrophobic/ hydrophilic	Fog harvesting	116
	PVDF/MWCNTs	Single-faced coating	Single-layer modification	Hydrophobic/ hydrophilic	Humidity stress sensor	139
Inorganic JMs	Copper foam	Femtosecond laser treated	Single-layer modification	Hydrophobic/ superhydrophilic	—	64
	Copper foam	Femtosecond laser treated	Single-layer modification	Hydrophobic/ superhydrophilic	Fog harvesting	58
Other JMs	Cu sheet, dodecanethiol and $(NH_4)_2 S_2O_8$	Alkali etching and soaking method	Single-layer modification	Superhydrophobic/ superhydrophilic	—	54
	Copper mesh, $(NH_4)_2 S_2O_8$ and FAS	Alkali etching and vapor deposition	Single-layer modification	Hydrophilic/ hydrophobic	Oil–water separation	53
	Copper mesh, $(NH_4)_2 S_2O_8$ and ODT/ethanol	Liquid modifications	—	Hydrophobic–hydrophilic/ hydrophobic	Fog harvesting	123
	Copper mesh, TiO_2 nanoparticles and dodecanethiol	Soaking method and UV-degradation	Single-layer modification	Superhydrophobic/ hydrophilic	—	110
	Copper mesh, $(NH_4)_2 S_2O_8$ n-tetradecyl mercaptan	Alkali etching and soaking method	—	Underwater superaerophobic/ aerophilic	—	111

(polydopamine/polyethyleneimine) solution surface. The PDA/PEI-modified layer was hydrophilic/superaerophobic (a contact angle greater than 150° to a small bubble in water) and the water drops were absorbed on this side, while the other layer still maintained hydrophobicity/aerophilicity (a contact angle smaller than 90° to a small bubble in water).

2.2.2 **Polymeric-inorganic Janus membranes.** Compared to polymeric Janus membranes, polymeric-inorganic Janus membranes combine easy processing, the flexibility of organic components and the mechanical properties of inorganic counterparts. They therefore have the potential to serve as building blocks for novel devices and materials.

12926 | J. Mater. Chem. A, 2019, **7**, 12921–12950

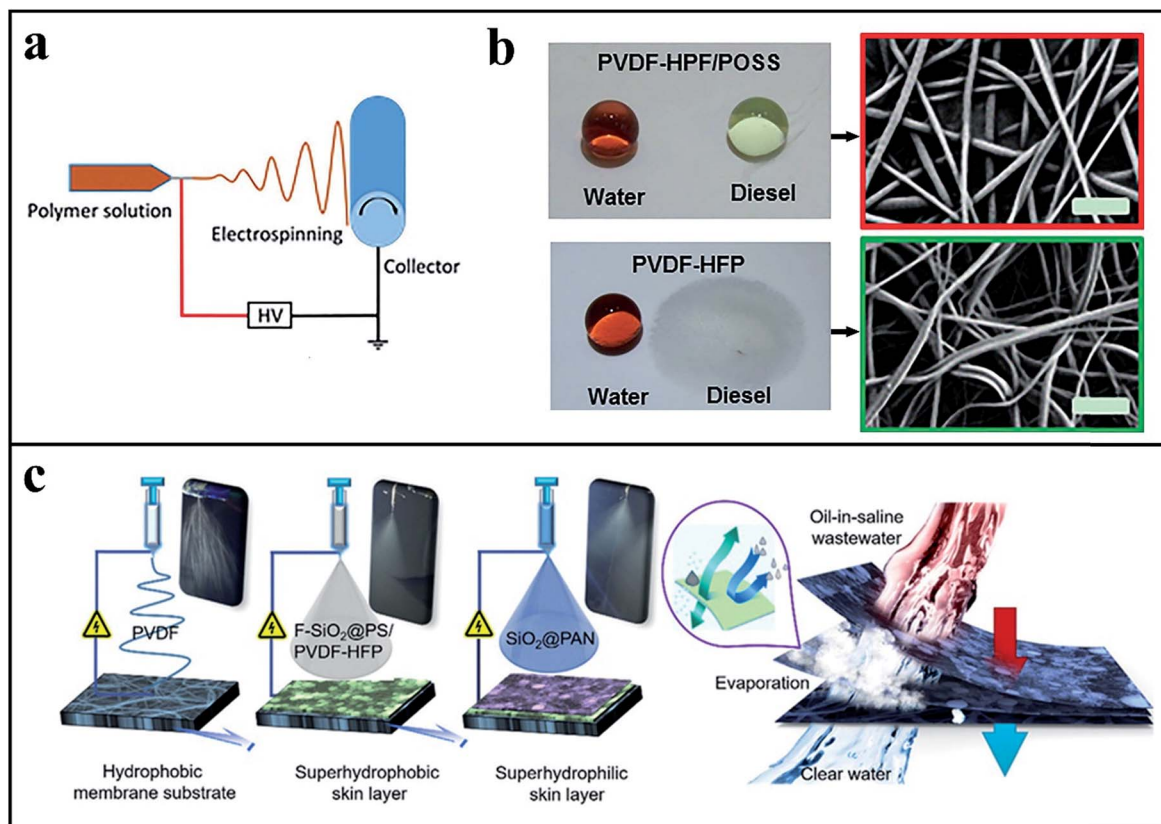This journal is © The Royal Society of Chemistry 2019

Fig. 4 (a) Schematic illustration of the electrospinning setup. (b) Photos of water and diesel droplets on the nanofiber membrane and SEM images of a dual-layer nanofiber membrane. Reproduced with permission.[62] Copyright 2015, Wiley-VCH. (c) Schematic illustration of the fabrication of the Janus skin layer with asymmetric superwettability on a necklace–structured PVDF NFM and the proposed mechanism of the antifouling and antiwetting properties using an asymmetrically superwettable Janus skin layer and a plausible mechanism of vapor permeation across the porous membrane. Reproduced with permission.[51] Copyright 2018, Elsevier B. V.

There is a popular method to prepare polymeric-inorganic Janus membranes, modifying the single-side of the membrane. For example, an emerging Janus membrane was prepared using a two-step coating technique and subsequent UV treatment.[63] As illustrated in Fig. 5a, this novel fabric was prepared first by coating flowerlike ZnO nanorods and FD-POSS/FAS, and then a single-side was irradiated with strong UV-irradiated light. When one side of the fabric was UV-irradiated for enough time, the UV-irradiated surface was hydrophilic, whereas the unirradiated side still maintained high superhydrophobicity.

It is unsuitable to use fluorine-containing materials to create hydrophobic surfaces due to the limitation of economic costs and the continuing serious environmental pollution. Therefore, it is necessary to develop inorganic materials to fabricate JMs. To this end, Yang et al.[52] in our group reported the example of fabricating JMs by sequential vacuum filtration. Moreover, vacuum filtration was subsequently used to construct a coating on the substrate membrane with tunable deposition amount. Fig. 5b shows that a series of JMs had been facilely fabricated by depositing superhydrophobic ZnO-Kevlar pieces on a hydrophilic FeOOH-Kevlar membrane via vacuum filtration. It was mentioned that a small amount of a mixture of FeOOH-Kevlar pieces and ZnO-Kevlar pieces with a ratio of 1 : 1 was added before adding ZnO-Kevlar pieces, with the aim of making the Janus membrane relatively tight. In brief, the process of melding modified side membranes was similar to the papermaking process. During the preparation process, two modified materials with opposite wettability were compounded which led to some ingenious phenomena when the liquid drops onto the membrane. As a result of this process, the treated FeOOH-Kevlar layer had been made greatly superhydrophilic, which was tested by measuring the water contact angle (WCA). Its WCA reached as low as $0°$, whereas the ZnO-Kevlar layer had nice hydrophobic properties, with the WCA rising to $142.1°$. Most interestingly, when changing the external medium from air to water, there was an oil contact angle of $152.9°$ on the FeOOH-Kevlar layer, presenting its superoleophobic characteristics. The ZnO-Kevlar layer showed superhydrophobic properties under oil with a WCA of $153.6°$. It should be noted that the composite Janus membrane had unusual properties of separating water-in-oil and oil-in-water emulsions with high separation efficiency. Besides, Si et al.[55] in our group prepared a Janus hydrophobic/superhydrophilic nickel foam via a simple floating strategy. The clear nickel foam was placed on the surface of starch paste ethanol dispersion and the nickel foam floated on the liquid surface (see Fig. 5d), because of the advantage of viscous starch paste dispersed in ethanol. The
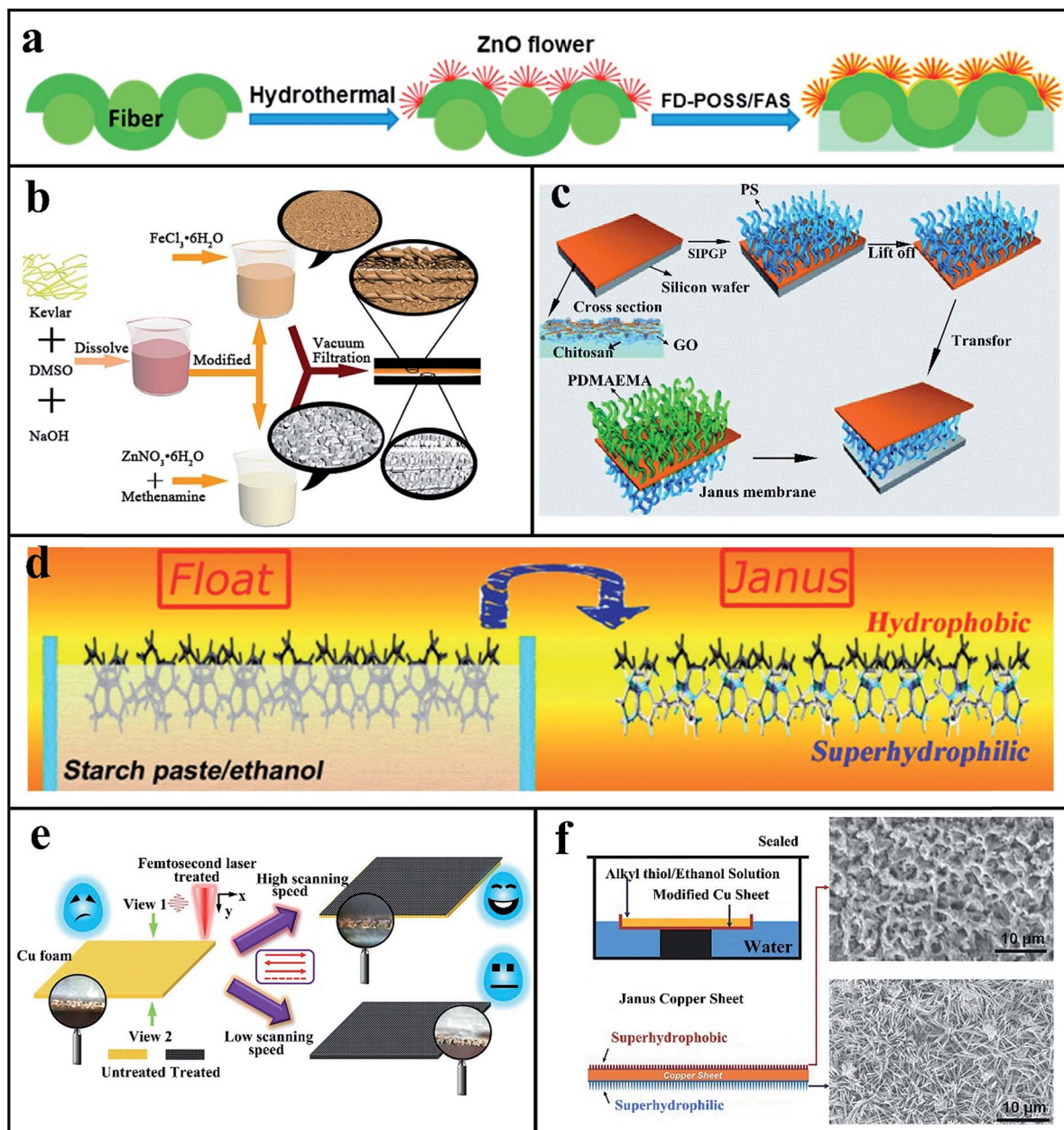
This journal is © The Royal Society of Chemistry 2019

J. Mater. Chem. A, 2019, 7, 12921–12950 | 12927

Fig. 5 (a) Coating procedure of Janus fabrics. Reproduced with permission.[63] Copyright 2015, American Chemical Society. (b) Fabrication of the modified Kevlar composite membrane for separation of oil–water emulsions. Reproduced with permission.[52] Copyright 2018, Elsevier B. V. (c) Schematic procedure of fabricating a polymer brush functionalized Janus graphene oxide/chitosan hybrid membrane. Reproduced with permission.[57] Copyright 2014, Royal Society of Chemistry. (d) Schematic illustration of the synthesis procedure of Janus nickel foam. Reproduced with permission.[55] Copyright 2018, Elsevier Inc. (e) Schematic diagram of the preparation, and characteristics of the Janus copper foam. Micro/nanostructures on the copper foam were formed using femtosecond laser ablation, and the ablation thickness could be controlled by the laser scanning speed. The magnified images in the inset are the corresponding cross-section ones. Reproduced with permission.[58] Copyright 2018, American Chemical Society. (f) The schematic diagram of the preparation of Janus sheets and the SEM images further demonstrate the morphologies of superhydrophobic and superhydrophilic surfaces. Reproduced with permission.[54] Copyright 2017, Wiley-VCH.

coated nickel foam formed a superhydrophilic surface, whereas the rest of the nickel foam in air still maintained its original hydrophobicity.

In addition to the aforementioned methods of fabrication of polymeric-inorganic Janus membranes, JMs can also be obtained by sequential single-side modification on each layer. For example, Han *et al.*[57] reported a polymer hybrid brush grafted

Janus graphene oxide (GO)/chitosan hybrid membrane. As shown in Fig. 5c, it was prepared by the combination of interface self-assembly of GO and chitosan, with subsequent self-initiated photografting and photopolymerization (SIPGP) from both sides of the GO/chitosan composite membrane. In detail, the GO/chitosan composite membrane was obtained firstly, and poly(styrene) (PS) and poly (*N,N*-dimethylaminoethyl

methacrylate) (PDMAEMA) were then grafted from the photo-active sites of the upper layer and lower layer of the GO/chitosan membrane by SIPGP, respectively.

2.2.3 Inorganic Janus membranes. Since JMs can be prepared by rapidly changing the surface topography, preparation using inorganic materials is the hottest research recently, and the resulting JMs are different from the above mentioned JMs containing polymer materials. For example, JMs can be obtained by femtosecond laser direct writing technology, which is a simple and low-cost method to rapidly fabricate nanoparticle covered microstructures on one side of an inorganic substrate.[64] As shown in Fig. 5e, an inorganic Janus membrane was prepared applying a one-step femtosecond laser scanning process, which had superior stability. Moreover, it should be noted that the treated surface possesses micro/nanostructures and exhibits superhydrophilicity, while the pristine surface exhibits hydrophobicity.[58]

The three types of JMs mentioned above only occupy a large proportion, and a small number of emerging JMs made from other materials appear, such as inorganic and organic substances. For example, an organic–inorganic Janus mesh membrane with unidirectional water transport ability was reported.[53] A copper mesh substrate was immersed into a water solution of NaOH and $(NH_4)_2S_2O_8$. After that, it could be seen that nanostructured Cu $(OH)_2$ had been produced onto the copper mesh substrate. After growth of the nanostructure, the membrane was covered on a beaker containing hydrophobic fluorosilane (FAS), and thus the FAS modified layer was hydrophobic, and another layer was hydrophilic. Interestingly, it could be found that the intensity of element F on the hydrophobic layer was remarkably higher than that on the opposite layer, revealing that the FAS molecules could penetrate into the copper mesh membrane.

At the same time, there is still a big challenge for synthetic JMs with a certain thickness due to capillarity. To this end, Zhao *et al.*[54] prepared a Janus sheet by distinguishingly modifying the two sides of a copper sheet with the aim of keeping the integrity and reducing the total thickness of the Janus sheet. It should be noted that the copper sheet was eroded by ammonium persulfate in an alkaline environment firstly. Single-side modification of the membranes is difficult to obtain through a wet coating process because of the capillary suction of the coating solution into the porous structure. Therefore, they used water as a protecting liquid for the superhydrophilic surface, and then took one side of the Janus copper sheet into the alkylthiol/alcohol solution (see Fig. 5f). As a result, the as-prepared Janus sheet not only had a superhydrophilic layer but also had a dodecanethiol-modified superhydrophobic layer. In short, many of the existing preparation methods have excellent performance but there are still some minor problems. Therefore, it is necessary to develop more preferable methods to fabricate JMs.

3 Unidirectional transport behaviors on Janus membranes

3.1 Wettability mechanism of Janus membranes

With the development of surface science, various superwetting materials, with characteristics including superhydrophobicity

(WCA> 150°)/superhydrophilicity (WCA ∼ 0°), super-oleophobicity (OCA > 150°)/oleophilicity (OCA ∼ 0°) or both simultaneously have been successfully prepared and applied in practice.[65] For lyophilic surfaces, it should be noted that when the droplets are dropped on the surface, they will spread immediately. However, for lyophobic surfaces, the wetting behavior of the droplets can be discussed in terms of conditions. In our group, using two kinds of low-cost, common and available vapours, we had achieved reversible regulation of the surface wettability and adhesive force of the hybrid MWCNT membrane from hydrophobic to superhydrophobic.[14] In addition, we also explored the theoretical reason behind this phenomenon. Meanwhile, several wetting regimes had also been reported for a hierarchical dual scale rough surface, including Wenzel, Cassie–Baxter, and impregnating Cassie wetting regime.[66] The use of Wenzel's theory explains the hydrophobicity of a homogeneous surface with roughness (Fig. 6a), which suggests that the surface roughness plays a crucial role in changing the wettability of the material.[67] In 1936, Wenzel took surface roughness into consideration and proposed the Wenzel equation for the homogeneous wetting regime described as follows:[67]

$$\cos \theta = r \cos \theta_0 \quad (1)$$

where θ is the contact angle of the rough surface, θ_0 is the Young's contact angle of the smooth surface, and r is the roughness factor defined as a ratio of actual to projected surface area. But this model does not explain the hydrophobicity of the roughness of the heterogeneous surface. On the basis of Wenzel's regime, once the water droplet is dripped to the hierarchical rough surface, water fills the pores completely. In addition, when $\theta_0 < 90°$, an increase in roughness will reduce θ, but if $\theta_0 > 90°$, an increase in roughness leads to an increase in θ. The relevant result is that the apparent contact area is much smaller than the real contact area with the surface adhesion between the liquid and surface being high. Therefore, the surface roughness can make the hydrophilic surface more hydrophilic, making the hydrophobic surface more hydrophobic, depending on the chemical composition on the material surface. In addition, the rough microstructure has the function of amplifying the wettability on the solid surface.[22,68]

When water droplets cannot permeate the pores of the rough surface, many trapped air pads exist at the solid–liquid interface (see Fig. 6b), enhancing the contact angle of the surface, and thus the contact angle of the surface can be calculated as:[69]
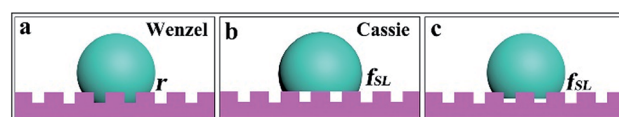

Fig. 6 Sketches showing the in-air wetting mechanism of water droplets residing on solid surfaces at different wetting states. Water droplets on rough surfaces with a homogeneous wetting state (a) and with a heterogeneous wetting state (b) and with a wetting state between them (c).

This journal is © The Royal Society of Chemistry 2019

J. Mater. Chem. A, 2019, **7**, 12921–12950 | **12929**

$$\cos\theta = f_{SL}\cos\theta_0 - 1 + f_{SL} \qquad (2)$$

where f_{SL} is the liquid–solid interface fraction. This Cassie–Baxter equation could satisfy the heterogeneous wetting regime situation. As a result, the apparent contact area is much bigger than the real contact area, and the surface adhesion between the liquid and surface is also low.[70]

Nevertheless, when water partially permeates the pores of the rough surface (see Fig. 6c), a contact angle is formed between Wenzel and Cassie wetting regimes and is calculated by:[71]

$$\cos\theta = 1 + f_{SL}(\cos\theta_0 - 1) \qquad (3)$$

Prashant Gupta et al.[72] had reported a Janus membrane with heterogeneous wetting properties, having the petal effect and ensuing impregnating Cassie wetting regime. Due to the porous nature and surface roughness of JMs, the hydrophobicity of JMs can be enhanced and even become superhydrophobic.[73] Therefore, it is possible to reduce the surface energy of the Janus membrane by modifying the surface with other materials to achieve the effect of enhanced hydrophobicity.[74,75]

3.1.1 Wetting transition and energy barriers. In order to construct an extreme wettability surface, it is vital to understand the influencing factors as well as the causes of the influence, and the typical one is the wetting transition mechanism.[76–78] Based on the above knowledge about wettability, when the wettability state changes from the Cassie–Baxter model to the Wenzel model, a process that overcomes the energy barriers, it is obvious that the wettability gradually decreases during this process. The energy coexisting between the liquid phase and the gas phase named the energy functional can be given by[78]

$$V(\varnothing) = \int_{\Omega}\left(\frac{1}{2}k|\nabla\varnothing|^2 + f(\varnothing)\right)dx \qquad (4)$$

where $\varnothing$ is an order parameter of the fluid, and $f(\varnothing)$ is a function of the energy density of the homogeneous phases, and it can be calculated as:

$$f(\varnothing) = \frac{1}{2}\varnothing^2(\varnothing - 1)^2 \qquad (5)$$

Two alternative phases can be explained with two minimum values of f: $\varnothing = 1$ in the liquid phase and $\varnothing = 0$ in the vapor phase. In addition, the thickness of the liquid–gas interface depends on $k : d = \sqrt{k}$. At the solid surface, the Dirichlet boundary condition is used for $\varnothing$:

$$\varnothing = \varnothing_s, \text{ and } 1 > \varnothing > 0 \qquad (6)$$

It is assumed that the total mass of the fluids during the wetting transition is invariable. Here, we impose the constraint

$$\int_{\Omega}\varnothing\,dx = C \qquad (7)$$

where Ω is the region occupied by the fluids and C is the mass of the fluids in the initial Cassie–Baxter state.

For the solid surface textured as a square lattice of rectangular pillars, there are many local minima through these equations. The wetting state, energy barriers and transitions can be calculated through the string method. The wetting transition occurs first in a single cavity on the solid surface, and then the liquid gradually reaches the bottom surface, as shown in Fig. 7. In summary, the surface structure plays a crucial role in the wetting transition. According to the above analysis, designing and manufacturing JMs with asymmetric wetting becomes easier and controllable.[79]

3.1.2 Porosity theory. Take the porosity theory as an example to discuss how to strengthen the mechanical properties of the membrane surfaces without being damaged. In addition, "needlelike" and "craterlike" structures are considered as the elements constituting a porous surface. Porosity can be defined as,[80]

$$\text{Porosity} = 1 - \frac{\rho_{membrane}}{\rho_{ref}} \qquad (8)$$

In the manufacturing process of porous JMs, mechanical properties hardness H and elastic modulus E must be considered, and E can be calculated using the following equation[81,82]
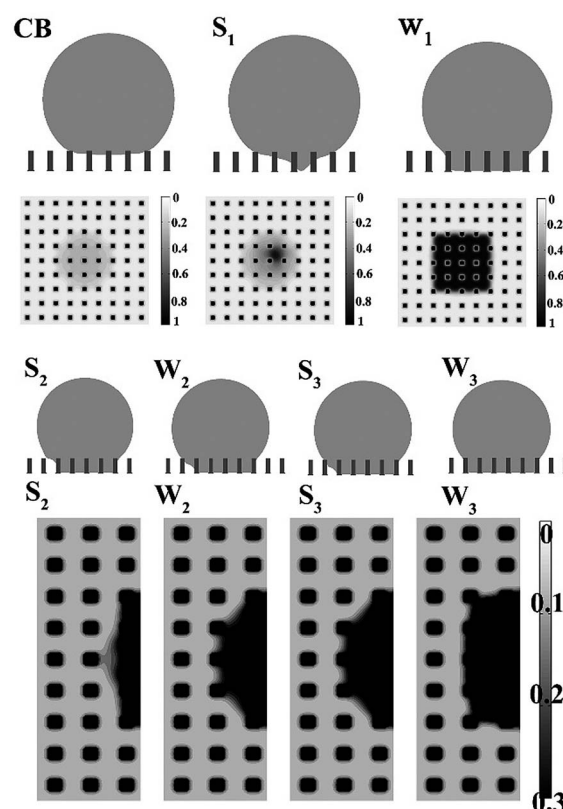

Fig. 7 Energy barriers for the Cassie-to-Wenzel transition: liquid permeates into the grooves on the substrate and undergoes lateral expansion, layer by layer. S_1 is the largest energy barrier and W_1 is a minimum wetted state. W_2 is an intermediate metastable state, and S_2 and S_3 are other energy barriers. Reproduced with permission.[78] Copyright 2014, American Chemical Society.

$$E_{\text{membrane}} = E_{\text{ref}} \left(\frac{\rho_{\text{membrane}}}{\rho_{\text{ref}}} \right)^n \tag{9}$$

where ρ is the density and n is related to the failure mechanism. The smaller-scale influences of structure and multiple mechanical properties can be achieved by adjusting through the following equation:[83]

$$\frac{A}{A_0} = (1 - \alpha p)^n \tag{10}$$

where A and A_0 are constant for membranes with a number of pores and nonporous membranes, respectively. α and n describe the packing geometry factor and the pore geometry, respectively. In order to analyze the relationship between diverse membrane properties, the following equation is introduced:

$$A_{\text{porous}} = A_0 \, e^{-bp} \tag{11}$$

where A_{porous} and A_0 are the properties of the porous membrane and nonporous membrane, respectively. b represents the performance of porosity and p describes the volume fraction porosity.

Based on these equations, it is obvious that the mechanical properties are inversely proportional to the power law of porosity. Therefore, we can adjust voids and porosity in JM surfaces to improve their life-times.

To sum up, the factors affecting the wettability, the mechanism for the Cassie to Wenzel transition and the porosity theory have been discussed in detail. According to these, it will be easier and more beneficial to prepare asymmetric wettability JMs that possess mechanical durability and stable chemical property.

3.2 Unidirectional fluid transport mechanism of Janus membranes

As mentioned above, the wetting of the water droplet just after it comes into contact with only one side of Janus membrane has been analysed in detail, but as time increases or as the accumulation of droplets becomes larger, directional transport of the liquid may occur. Compared to the movement of droplets on the surface, this whole process is further complicated for the unidirectional transport behaviors taking place in the direction of the cross section of the Janus membrane. Generally, directional transport of liquids can be divided into two types. One is the movement that occurs on the surface. Interestingly, this phenomenon exists in nature, such as the surface of butterfly wings[84] and the collection of water from spider silk.[85] The other is the movement that occurs in the cross-section direction, and the liquid that directionally transports on the Janus membrane follows this way. Recently, there have been relatively more reports on JMs, especially the study of unidirectional transport behavior on JMs. Tian et al.[86] constructed a simple model of a membrane consisting of microcylinders, theoretically showing a membrane with a cross-sectional wettability gradient and anisotropic liquid penetration. As shown in Fig. 8a, it can be clearly seen that the liquid can penetrate from the lyophobic side to the lyophilic side, while the liquid is directly blocked and has almost no penetration in the opposite direction. For JMs, unidirectional fluid transport is often driven by opposite wettability on two sides, using the wetting gradient on the cross-section to provide the driving force. In nature, it is interesting that the desert beetles collect water from the atmosphere using the hydrophilic knots on the hydrophobic surface.[87] Inspired by similar phenomena, a large number of JMs were successfully prepared to verify the unidirectional transport of liquids. Liu et al.[88] constructed a two-dimensional (2D) Janus fabric with anisotropic wettability via electrospraying, a facile and conventional technique. In their work, transport behaviors of water droplets and oil droplets on the 2D Janus fabric are depicted. When the fluid came into contact with the lyophobic side, it passed through the membrane and then began to spread on the other side, while it spread on the lyophilic side without any permeation. Therefore, the transmembrane pressure from the hydrophobic side is much lower than that from the hydrophilic side. Moreover, many researchers have also converted the theoretical model of unidirectional transport of liquids on the Janus membrane into an implementation that has been successfully verified experimentally.

Furthermore, our group also discovered unidirectional water transport in a hydrophilic–hydrophobic Janus nickel foam.[55] However, the phenomenon that the water droplet transports from one side of the Janus membrane to the other side can be directly observed, whereas it is difficult to visually analyse the detailed directional transport process of the liquid and the principle of transportation. Therefore, unidirectional liquid transportation can only be analysed from the whole, exploring the specific transport principle. Si et al. analysed the system of the prepared Janus foam nickel and a water droplet.[55] The mechanism of unidirectional liquid transportation is depicted in Fig. 8c. For the hydrophobic layer upwardly situation, when a water droplet is placed on the hydrophobic side, it suffers two opposite forces. One is hydrostatic pressure (F_G) due to the force of gravity, which is thought to be the reason for the unidirectional water transport, and the other one is hydrophobic force (F_H). In the beginning, F_G and F_H will keep balance. Whereas, when the F_G is large enough, it can overcome F_H, making water reach the hydrophilic layer. Once water arrives at the superhydrophilic layer, the F_H becomes zero. At this moment, the capillary force (F_C) within the hydrophilic side appeared, assisting the water spreading in every possible direction within the hydrophilic layer. In contrast, for the hydrophilic layer upwardly situation, when water is dropped onto the hydrophilic layer, it gets absorbed easily due to F_C, resulting in a negligible F_G on the hydrophobic layer. F_C and F_G make water transfer to the hydrophobic layer and F_H, can offset the resultant force ($F_C + F_G$), resulting in water being stopped from permeating further. It is quite clear that F_C plays a vital role in achieving unidirectional liquid transportation of Janus materials.[16,89] However, these theoretical explanations are not completely convincing, and seeking methods to actually quantify the force (F_H, F_C and F_G) will be a meaningful research focus for JMs. In this system, F_H generated by the hydrophobic layer preventing liquid from penetrating can also be described as "breakthrough pressure ($F_{\text{breakthough}}$)". When F_G is equal to or

This journal is © The Royal Society of Chemistry 2019

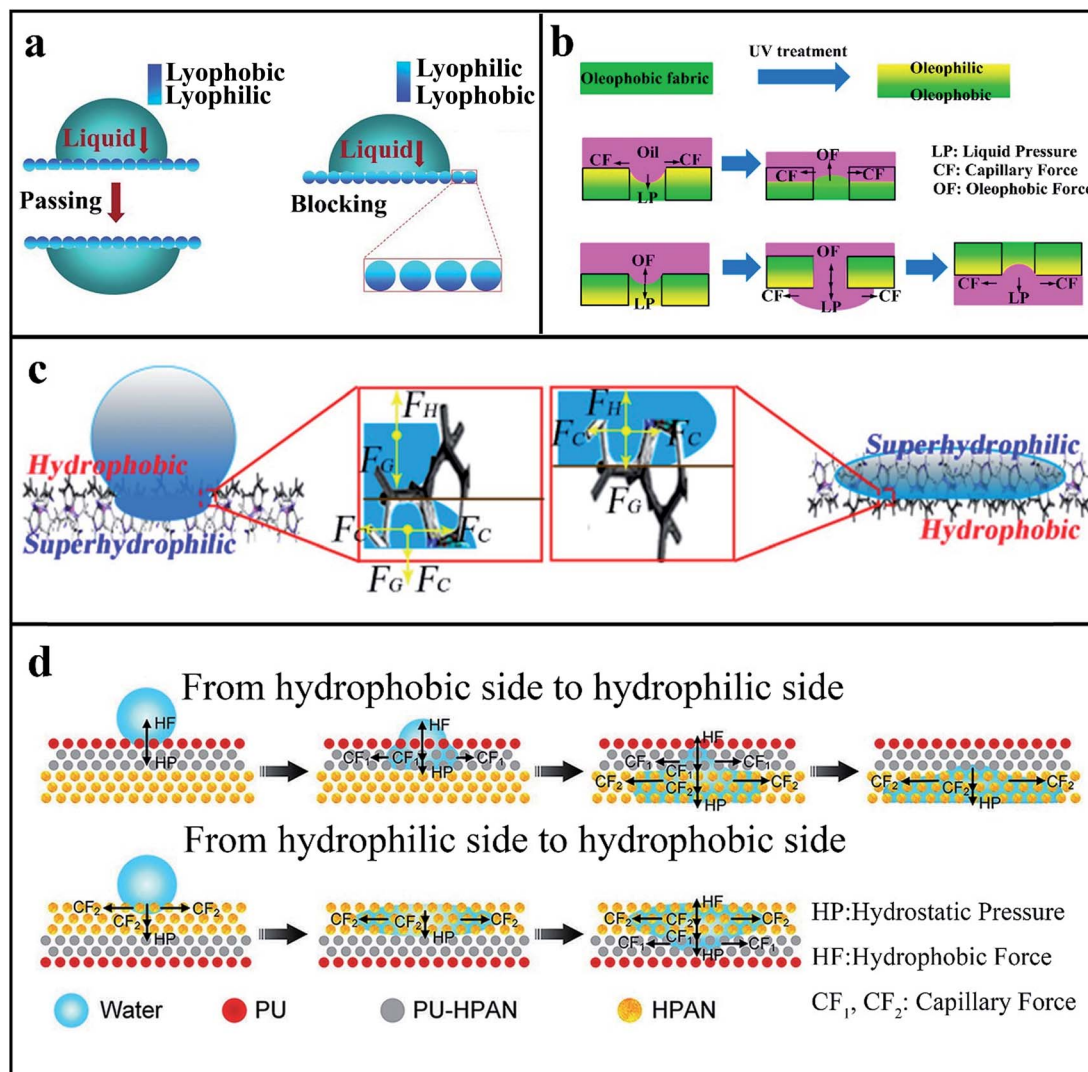J. Mater. Chem. A, 2019, 7, 12921–12950 | 12931

Fig. 8 (a) Anisotropic liquid penetration through a microcylinder membrane with a wettability gradient along its thickness. (a-left) The liquid penetrates easily in the positive direction (lyophobic side/lyophilic side). (a-right) The liquid is blocked in the reverse direction (lyophilic side/ lyophobic side). Reproduced with permission.[86] Copyright 2012, Royal Society of Chemistry. (b) Proposed one-way oil-transport mechanism. Adapted with permission.[63] Copyright 2015, American Chemical Society. (c) The schematic of the mechanism of the directional water transport on Janus nickel foam. Adapted with permission.[55] Copyright 2018, Elsevier Inc. (d) Schematic illustration of the unidirectional water transport mechanism: water is dropped on the upward hydrophobic PU side and HPAN side, respectively. Reproduced with permission.[45] Copyright 2018, Wiley-VCH.

more than $F_{breakthough}$, water can still penetrate the Janus nickel foam from the superhydrophilic to the hydrophobic layer. It seems to be reasonable to use the maximum water column height to represent $F_{breakthough}$, and thus $F_{breakthough}$ can be expressed as[40,90,91]

$$F_{breakthrough} = -\frac{2\gamma}{r} \cos \theta \qquad (12)$$

where θ is the contact angle between the hydrophobic layer and the water, γ is the surface tension, and r is the pore radius. According to this equation, when the pore size becomes larger or the contact angle becomes smaller, the Janus nickel foam would not support a high water column.

It is worth noting that the oil droplet shows similar directional transport behavior on JMs. The reported JM for oil

unidirectional permeation is generally oleophobic–oleophilic (solid surface with a static oil contact angle $\theta > 90$ or $\theta < 90°$) rather than hydrophobic–hydrophilic because the hydrophilic surface is also oleophilic in air.[62,63] However, it becomes oleophobic underwater in most cases, and the hydrophilic–hydrophobic Janus membrane may exhibit unidirectional oil transport underwater. Similar to the unidirectional transport mechanism of water on a Janus membrane with a wetting gradient across the thickness, the one-way oil-transport mechanism was also put forward.[63] As demonstrated in Fig. 8b, after UV-treatment, the wettability of one side of the fabric changes from oleophilic to oleophobic. As a result, once oil droplets are dripped on the oleophilic side, they can spread rapidly, and the penetration phenomenon cannot occur due to the high oleophobicity of the lower layer. Conversely, when oil droplets come

into contact with the oleophobic surface, they will overcome the barrier of the oleophobic layer and smoothly penetrate from one side to the other.

Much of the research on unidirectional liquid transportation on JMs has focused on bilayered structures with controlled thickness and different wettability on the upper and lower sides.[89,92,93] However, these double-layered JMs still have certain limitations for unidirectional liquid transport, and they are still imperfect for controlling the continuous transport of liquids in the positive direction and preventing the directional transport in the opposite direction. Obviously, new Janus membranes that can overcome these problems still need constant research. For example, a trilayered hydrophobic/transfer/superhydrophilic fibrous membrane was prepared and the unidirectional liquid transportation mechanism above was also discussed in detail (see Fig. 8d).[45] When water droplets are dropped on the trilayered Janus membrane, unidirectional transport behavior occurs in the air–water system. Similarly, water droplets can penetrate the Janus membrane from the hydrophobic layer to the intermediate layer and then spread on the hydrophilic layer, whereas the directional transport behavior will disappear and the water droplets will be prevented from penetrating in the opposite direction. In order to explain the reason for this phenomenon, there is a simple model that can clearly describe the

unidirectional transport behavior and the systematic physical mechanism in Fig. 8d.[45] Here are some forces that do not change in the direction of the water droplet, including the hydrophobic force (HF), hydrostatic pressure (HP) due to the height of the water droplet and the capillary force (CF_2) generated by a super-hydrophilic surface. Similar to the mechanism on the bilayered Janus membrane, a capillary force (CF_1) is added here from the intermediate layer. When the droplets move from the hydrophobic layer to the hydrophilic layer, this force promotes liquid transport, whereas this force hinders directional liquid transport in the opposite direction. This Janus membrane not only improves the unidirectional transport behavior of the liquid droplets, but also enhances the moisture wicking performance.

In the above case, gravity has always been the driving force in the unidirectional liquid transportation process, which promotes the movement, but how does the liquid move when gravity becomes the resistance? Studies have shown that the antigravity liquid spontaneous unidirectional transport behavior can proceed smoothly.[64,94] For example, the antigravity unidirectional transportation of water droplets on the Janus membrane can be analysed in detail by a mechanism, which can be seen in Fig. 9b.[64] There are three forces acting on the water droplet, including gravity (F_G), adhesion force (F_A) and capillary force (F_C), and when the resultant force of the three
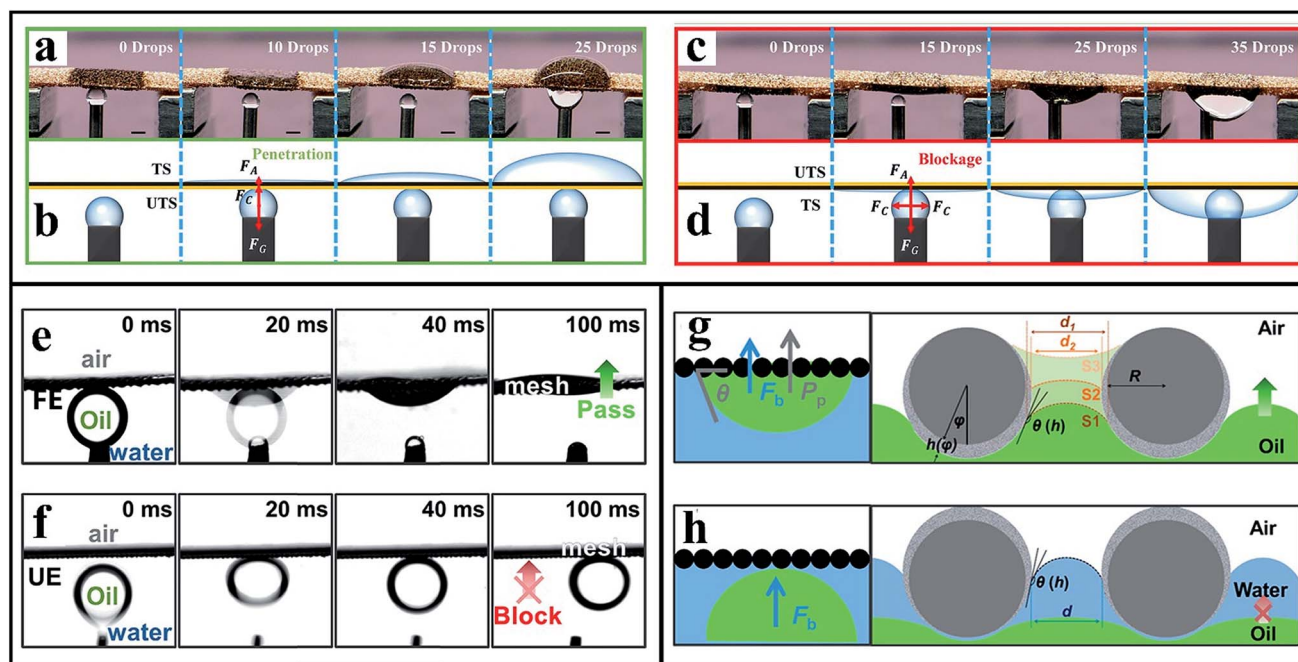

Fig. 9 Water antigravity unidirectional transport on the Janus foam. (a) Sequence of digital photographs showing the upward penetration of water through the Janus foam, and transfer from the UTS to TS. (b) Mechanism diagrams corresponding to the photographs in (a). (c) Sequence of digital photographs showing the downward penetration of water being blocked by the Janus foam, so that it cannot transfer from the TS to UTS. (d) Mechanism diagrams corresponding to the photographs in (c). Reproduced with permission.[64] Copyright 2018, American Institute of Physics. Directional oil penetration in an air–mesh–water system. (e) Gradient mesh with Janus wettabilities allows penetration of the under-water n-hexadecane droplet when the fire-exposed side (FE) is toward water. (f) When the unexposed side (UE) of the mesh is toward water, the n-hexadecane droplet is blocked. (g) Schematic diagrams demonstrate that oil rapidly penetrates through the mesh and spreads on the other side of the mesh, when floating the gradient mesh with fire-exposed side (FE) down. (h) Schematic diagrams demonstrate that the oil phase is repelled from wetting the micro/nanostructured mesh by a thin layer of water, when floating the gradient mesh with the unexposed side (UE) down. Fluorescence emission from water and oil is shown in blue and green, respectively. Reproduced with permission.[94] Copyright 2018, American Chemical Society.

This journal is © The Royal Society of Chemistry 2019

J. Mater. Chem. A, 2019, 7, 12921–12950 | 12933

forces is upward, the water droplets will be transported in one direction, from the lower hydrophobic layer to the upper hydrophilic layer (see Fig. 9a). However, the direction of the capillary force changes as the direction of the Janus membrane is reversed, spreading along all directions of the hydrophilic layer, so that the unidirectional transport of the water droplets cannot occur (shown in Fig. 9d).

Interestingly, oil droplets also have similar transport behavior. For example, the oil droplet rapidly penetrates through the Janus mesh from the fire exposed layer (FE) to the unexposed layer while it can be blocked and still keep a sphere shape by turning over the Janus mesh (see Fig. 9e and f).[94] It should be noted that the upper and lower sides of the Janus membrane have different wettability under different environments, *i.e.*, in air super-oleophobicity of the fire-exposed mesh surface and oleophilicity of the unexposed surface and underwater oleophilicity of the fire-exposed surface and superoleophobicity of the unexposed surface. As illustrated in Fig. 9g, there is a detailed mechanism which can explain such an antigravity transport behavior. Unlike the previous analysis, this unidirectional transport behavior occurred in the air–oil–water–solid four-phase, which was visualized and demonstrated for the first time through laser confocal microscopy. During the unidirectional oil transportation process, there are both a large Young–Laplace pressure P_P on the Janus mesh and a buoyancy force F_b on the oil droplet, which can jointly drive the oil droplet to spontaneously move. However, when the Janus mesh was turned over, the Laplace pressure almost disappeared, leaving only the buoyancy force, not enough to drive the oil droplet directional transport (Fig. 9h).[94]

The unidirectional transport properties of the liquid can be applied in practice, such as oil–water separation, emulsion preparation and water collection, with higher efficiency than conventional methods, and the driving force provided by the inherent asymmetric wettability can also reduce energy consumption. The most special thing is that the upward delivery using the special property of JMs is convenient in daily life and industry. Therefore, it is necessary to continuously analyse the specific unidirectional transportation behavior and apply it to more practical applications.

3.3 Unidirectional gas bubble transport mechanism of Janus membranes

It is well known that gas bubbles are easily present in aqueous medium, which still poses challenges in commercial applications, including the pipe transportation of fluid[95,96] and control of the foaming process.[97] Therefore, it is meaningful to study the unidirectional transport of gas bubbles. Under normal circumstances, buoyancy is the only force of bubble motion without external force, having little effect on microscopic bubbles. Inspired by unidirectional liquid transport, introducing the gradient of the Laplace pressure and surface free energy can improve efficiency. The wetting gradient is the necessary condition for the unidirectional transport behavior of the gas bubble on the surface or in the cross-section direction of membranes, helping to promote the movement of bubbles. Next, we will explore unidirectional gas bubble transport from

two aspects, including surface and cross-section direction movements.

3.3.1 Directional transport of bubbles in the surface of the common membranes. For the solid surface immersed in water, different wetting states between the surface and the liquid film are vital to the adhesion of gas bubbles on the surface. When the superhydrophilic surface is placed in water, the pores on the surface can be filled with water immediately and the gas bubbles have little chance to come into contact with the solid surface. As the gas bubbles grow larger, it is easy for gas bubbles to detach from superhydrophilic surfaces, whereas they could adhere and spread over superhydrophobic surfaces.[98] From Fig. 10a, it can be clearly seen that the adhesion state and shape of the gas bubble on the surface of different wettable solids are very different, including the spread state, hemispherical and spherical state.[99] Interestingly, it has been experimentally demonstrated that the same superhydrophobic membrane can be used to have different properties for gas bubbles underwater by changing the experimental conditions.[100] As shown in Fig. 10b, the superhydrophobic membrane can be reversibly converted into underwater superaerophilic (a contact angle smaller than 10° to a small bubble in water) and underwater superaerophobic by underwater vacuumizing treatment. The next discussion mainly focuses on the directional gas bubble transport behavior on hydrophobic surfaces. To the best of our knowledge, due to the difference in surface tension, fine gas bubbles would merge with large bubbles so that large bubbles tend to become larger, and smaller bubbles become smaller. On a solid surface, large bubbles could quickly detach from the surface and rise due to the increased buoyancy.[101] The group of Jiang[102] has proved that spontaneous and directional transportation of gas bubbles on superhydrophobic cones could be realized. However, when the surface is fixed horizontally, the directional transport of gas bubbles may not occur. And how does the gas bubble move specifically on the solid surface which is placed horizontally? Taking a 3D porous copper wire with superhydrophobicity as an example, directional gas bubble transport behavior in the aqueous medium was studied in detail.[103] Some results exhibit that the low surface energy of the 3D surface leads to its ability to capture and directionally transport gas bubbles and it is very interesting that directional transportation is always towards to the larger bubble, as illustrated in Fig. 11a. Generally, gas could easily fill into the porous surface in a gaseous atmosphere.[104] Once the porous super-hydrophobic membrane is placed in the water atmosphere, the pore structures above will be filled with gas, resulting in increased surface tension. The gas film around the surface is formed by the combination of the hydrostatic pressure, entrapped gas Laplace pressure, atmospheric pressure, and the surface tension.[105,106]

At the gas–liquid interface, there is a Laplace pressure difference ΔP.

$$\Delta P = \frac{\gamma}{R} \tag{13}$$

where γ is the tension and R is the curvature radius of the gas–liquid interface. When the gas bubbles begin to come into
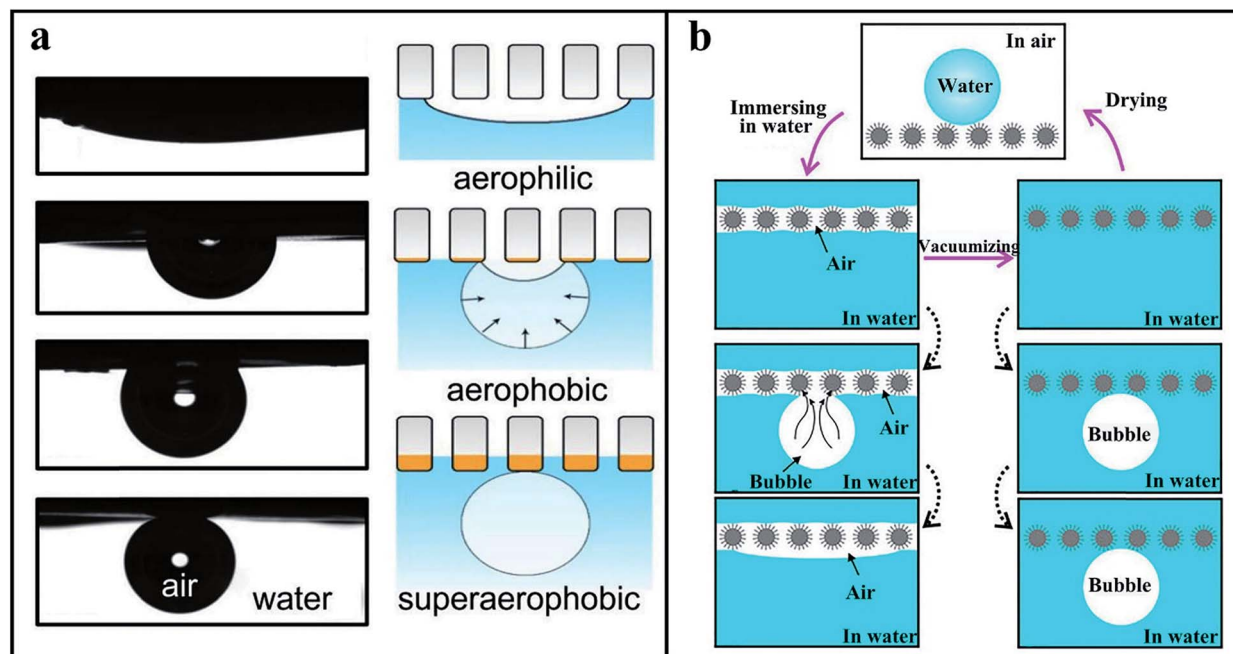
Fig. 10 (a) Photographs and schematic diagrams of different states of underwater bubbles on different wettability surfaces. Reproduced with permission.[99] Copyright 2018, Wiley-VCH. (b) Schematic illustration of the switch between underwater superaerophilicity and underwater superaerophobicity. (b-top) Water droplet on the as-prepared mesh (after drying) in air. (b-left) Immersion of the mesh in water. (b-right) The wetting of the as-prepared mesh that was immersed in water and further subjected to vacuumizing treatment. Adapted with permission.[100] Copyright 2018, American Institute of Physics.
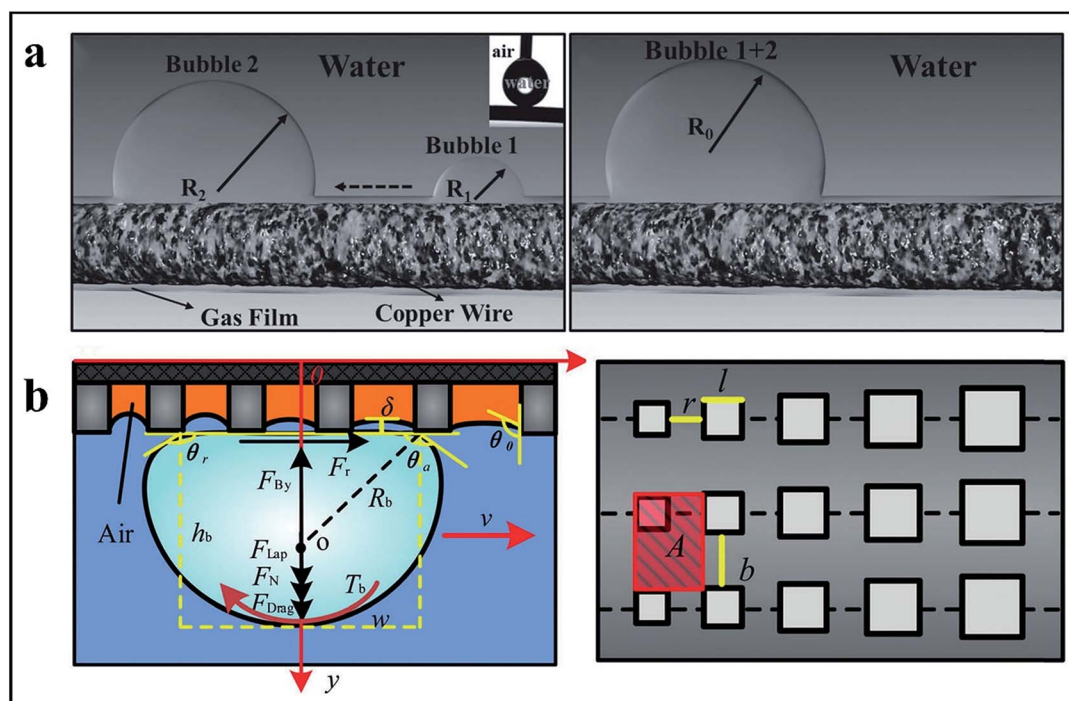

Fig. 11 (a) Mechanism of directional gas collection on copper wire. Reproduced with permission.[103] Copyright 2015, Wiley-VCH. (b-right) The diagram on the right one shows the real image of the fabricated surface and the surface structures, which are specified by a series of parameters. (b-left) The force analysis of underwater bubbles. The magnification of an arbitrary microhole on the surface shows the force analysis of the wrapped water (the orange section represents the air in the microhole). Adapted with permission.[107] Copyright 2018, Royal Society of Chemistry.

contact with the surface, they will be immediately captured by the gas film, resulting from the difference in pressure between the gas bubble and the gas film. The relationship between the Laplace pressure ΔP_b on the bubble and the radius of curvature R_b can be calculated as:

$$\Delta P_b = \frac{2\gamma}{R_b} \tag{14}$$

Considering eqn (13) and (14), if $R_b > 2R$, there exists a relationship that is $\Delta P_b < \Delta P$, indicating that the gas film had a larger Laplace pressure than the gas bubble. Conversely, there is an interesting phenomenon that the gas bubbles would be absorbed by the gas film. The buoyancy of gas bubbles will maintain balance with the Laplace pressure, once the link is formed between the gas bubble and the gas film. After that, the gas bubble could maintain stably a spherical crown shape on the surface. The radius of the spherical crown shape bubble (R_S) can be calculated by the followed equation.

$$R_S^2 = \frac{6\gamma}{\rho g} \frac{\tan^2 \theta/2 (1 + \tan^2 \theta/2)}{1 + 3 \tan^2 \theta/2} \tag{15}$$

As can be seen from the above information, the smaller bubble had larger Laplace pressure than the larger one. So that the small one tends to be transferred to the large bubble directionally. In addition, it should be noted that only a tiny size difference between two bubbles can produce the transportation.[103]

As for the cause of bubble motion on the surface above mentioned, it is mainly caused by the directional merge of adjacent bubbles rather than the self-driven motion of the single bubble. Chen and co-workers fabricated a polydimethylsiloxane (PDMS) surface with microholes in different sizes, which can promote the directional motion of gas bubbles in the water atmosphere.[107] When one bubble begins to come into contact with the as-prepared surface, there are forces acting on the underwater bubble, including the drag force F_{drag} from the surrounding liquid, the buoyancy force F_{By}, the elastic force F_N from the hydrophobic surface and the Laplace force F_{Lap} (shown in Fig. 11b). The Laplace force F_{Lap} could be calculated by the following equation.

$$F_{Lap} = \Delta P_b A_{LG} = \frac{2\sigma_L}{R_b} \frac{\pi}{4} w^2 = \frac{\pi \sigma_L w^2}{2R_b} \tag{16}$$

where ΔP_b is the Laplace pressure on the bubble, w is the width of the contact area and A_{LG} is the area between the bubble and the surface.

For the buoyancy force F_{By}, it is proportional to the total volume V_b and increases with it. It can be expressed as

$$F_{By} = \rho_L V_b g \tag{17}$$

where

$$V_b = \frac{4}{3} \pi R_b^3 \tag{18}$$

Therefore, the buoyancy force F_{By} is

$$F_{By} = \frac{4\pi}{3} \rho_L g R_b^3 \tag{19}$$

The drag force F_{drag} is given by

$$F_{drag} = C_D \frac{\rho_L U_\infty^2}{2} \pi R_b^2 \tag{20}$$

where U_∞ is the velocity of the gas bubble relative to the fluid and C_D is the drag coefficient determined by the Reynolds number Re, which was put forward by literature studies.[108,109] Under the combined effect of these forces, self-transport gas bubbles can be obtained, which may expand their practical applications.

3.3.2 Unidirectional transport of bubbles in the cross-section direction of Janus membranes. Another type of directional bubble transport occurs on JMs with asymmetric wettability resulting from the wetting gradient in the cross-section direction. Due to the driving force provided by the wetting gradient, resources can be effectively saved, and the gas bubbles can also be transported more easily, which lays a foundation for the directional manipulation of the gas bubbles. Therein, a Janus mesh with significant wettability difference between its two sides was produced by Chen and co-workers,[110] and it had large pores to facilitate underwater air transport. Note that as the air film is formed on the hydrophobic layer and the water film is formed on the hydrophilic layer, the asymmetric wettability Janus membrane has different attraction and repulsion force for gas bubbles in the water medium. The hydrophobic layer further turns into an aerophilic layer, while the hydrophilic layer turns into aerophobic layer. Underwater and unidirectional gas penetration could be effectively achieved on JMs. Similar to the unidirectional liquid transportation at the gas–solid interface, gas bubbles can also be directionally transported in aqueous media whether the Janus mesh is placed horizontally or vertically. Under the action of buoyancy and Laplace force, the underwater gas bubbles would transport from the aerophobic layer to the superaerophilic layer spontaneously once the bubbles were placed on the aerophobic side of the Janus membrane, whereas they would spread horizontally and be blocked by the opposite direction (shown in Fig. 12a).[110] Comparing the transport of gas bubbles on the hydrophobic membrane and the Janus membrane, it is found that when gas bubbles pass through the hydrophobic membrane, they are enlarged in a hemispherical shape, whereas they are spherically enlarged on the Janus membrane, so that the final bubble on the Janus membrane is much smaller than the former (shown in Fig. 12b).[56]

In the liquid medium, the buoyancy of the gas bubble is always upward. When the gas bubble moves from the bottom to the top, the buoyancy is the driving force. When the bubble moves from the top to the bottom, the buoyancy becomes the resistance so that the gas bubble is more difficult to perform the directional movement. Pei et al.[111] composited a Janus mesh for underwater bubble anti-buoyancy unidirectional penetration, which was different from the mentioned above that the
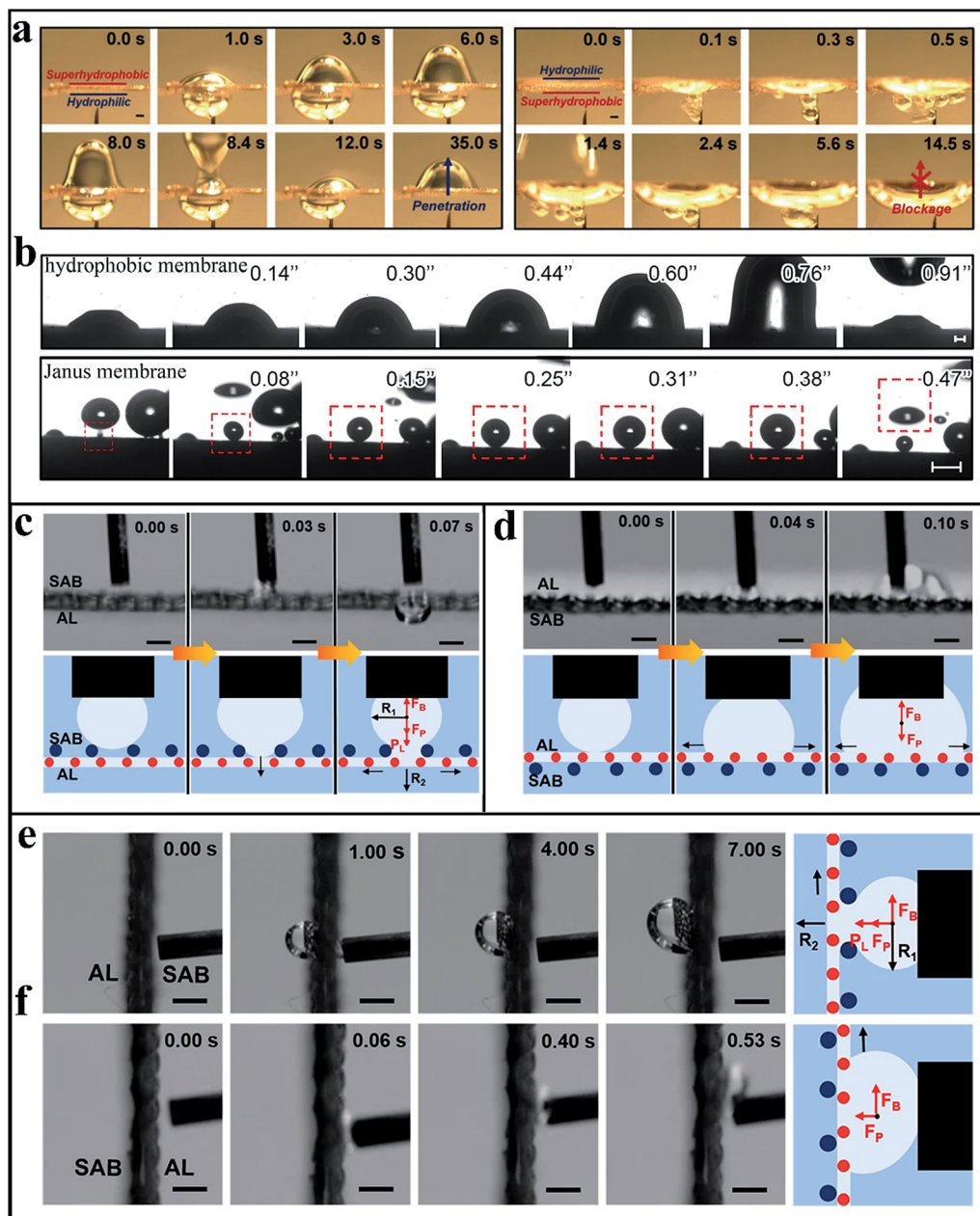
Fig. 12 The tests on the underwater unidirectional air penetration on this air "diode". (a) The air bubble can easily pass through the Janus mesh from the hydrophilic side, whereas it will be blocked from the superhydrophobic side. Reproduced with permission.[110] Copyright 2015, Royal Society of Chemistry. (b) The process of bubbling through the nascent and Janus membranes. Reproduced with permission.[56] Copyright 2016, Wiley–VCH. Underwater bubble unidirectional penetration on a composite mesh fixed vertically in water. (e) The bubble readily passes through the composite mesh from the superaerophobic (SAB) side to the aerophilic (AL) side. (f) The bubble is blocked from the aerophilic side. Untagged arrows in the schematic indicate the bubble's moving/spreading direction. Reproduced with permission.[111] Copyright 2018, American Chemical Society.

buoyancy facilitated gas bubble transport, expanding its applications in practice. During the underwater gas bubble unidirectional penetration process, the pore size of the superaerophobic layer plays a decisive role and only when the pore size of the superaerophobic layer is within the appropriate range, the pore diameter of the aerophilic layer can be neglected. It is convenient for the as-prepared Janus mesh to exhibit favourable underwater gas bubble transportation by adjusting the pore size of the Janus membrane. As illustrated in Fig. 12, a mechanism is studied to interpret the unidirectional penetration behavior of the underwater gas bubbles.[111] Comparing with the principle discussed above for the hydrophobic surface, it was found that the Janus membrane only increases the driving force provided by the wetting gradient in the cross-section direction, i.e., the Laplace force. When the gas bubble comes into contact with the superaerophobic side of the Janus

This journal is © The Royal Society of Chemistry 2019

J. Mater. Chem. A, 2019, 7, 12921–12950 | 12937

mesh, it may gradually deform and cross through the Janus membrane, which generates a channel between the gas bubble and under-gas layer. Therefore, there is a differential Laplace pressure P_L in the gas phase because of the different radius of curvature between the gas bubble and the lower aerophilic gas layer. This phenomenon can be explained by the Young–Laplace equation,

$$P_L = \gamma \left(\frac{1}{R_1} - \frac{1}{R_2} \right) \tag{21}$$

where γ is the surface tension of water, R_1 is the radius of curvature of the bubble and R_2 is the radius of curvature of the gas film. As shown in Fig. 12c, there are two forces playing crucial roles in the process of unidirectional gas transportation, including the pressure of the syringe pump and the Laplace pressure difference. When the combined force of the Laplace pressure (P_L) and the pump force (F_P) is greater than the buoyancy of the bubble (F_B), the gas bubble can be transported from the superaerophobic side to the aerophilic side. In contrast, it spreads on the aerophilic layer and cannot penetrate through the Janus mesh once the gas bubble comes into contact with the aerophilic side due to the disappeared P_L between the gas bubble and superaerophobic side (see Fig. 12d). At this time, only if there is a large external pressure can the directional transport behavior of the bubble be realized. Besides, underwater bubble unidirectional penetration in circumstances where the Janus mesh is orientated vertically in water can also be achieved (see Fig. 12e). Similarly, the diode transporting behavior disappears and the gas bubbles begin to float on the water surface (see Fig. 12f), when the aerophilic side of the Janus mesh is placed toward the gas bubbles. These results indicate that the as-prepared Janus mesh can be placed either vertically or horizontally, which has little effect on the passage of gas bubbles.

4 Applications

4.1 Fog collection

In the past few years, the pollution of water has become worse in many parts of the world, which is a research hotspot due to the water shortage.[112,113] It should be noted that fog, the micrometer-scale water droplets existing in air with a radius ranging from 1 to 10 μm, is among the most commonplace objects in our daily life.[114] In nature, there are lots of creatures equipped to harvest water due to their microscopic structures on their surface.[115] A typical example is spider silk, which has a periodic joint/spindle-knot structure, showing unique ability to collect tiny water drops from air.[85] And the Namib Desert beetle collects water from air through its rugged back composed of hydrophilic nonwaxy regions and hydrophobic waxy regions.[87] In addition, other natural creatures also use their own characteristics to collect water.

Inspired by the Namib Desert beetle with a water harvesting ability, a large quantity of hydrophobic–hydrophilic membranes emerged in response to the needs of water collection. As research on water collection proliferated, all kinds of methods were proposed by researchers, as well as they began to fabricate heterogeneous wettable JMs to collect water. JMs exhibited a marvelous water collection ability by adsorbing tiny water droplets on the hydrophilic layer while facilitating the removal of water droplets with the help of the hydrophobic layer.

In the meantime, collection devices can also be divided into many types. For example, a hydrophobic/hydrophilic cooperative Janus system was reported by Cao and co-workers.[116] In the first place, a Janus system was generated by tightly combining the as-prepared hydrophobic mesh and hydrophilic cotton absorbent. More meaningfully, a further designed 3D cylinder Janus collector as a potential fog collection apparatus was obtained by turning the 2D Janus membrane into the 3D fog collector with a cylinder shape due to the boundary layer effect. The collector with desirable properties exhibited a continuous process of efficient collection, unidirectional transportation and rapid spontaneous preservation of collection water. Furthermore, the rapid water droplet delivery of the Janus system could not only regenerate the fresh surface for fog collection, but also reduce the evaporation rate of the collected water.

Based on previous research, effective fog collectors should satisfy some requirements:[116] a relatively hydrophobic surface, rapid transport of water, fresh surface which can be continuously generated, and lower re-evaporation rate of water. According to these necessary features, Ren et al.[117] demonstrated a single-layer Janus membrane with dual gradient conical micropore arrays for effective collection. Furthermore, the special morphology of conical pores and asymmetric wettability generated the self-driving force which could help the water droplets transfer from the top side to the bottom side. The fog collection ability of the Janus aluminum membrane compared with superhydrophobic and superhydrophilic ones was further analyzed, and it was found that the Janus membrane had the highest collection rate and possessed a 209% enhancement in water collection compared with superhydrophilic membranes.

Compared with membrane desalination technology, which has been applied to make fresh water, fog is a unique water resource.[118,119] However, this technology also has problems since the harvesting process does not provide all-weather, full time operation and fast production on artificial nanostructure surfaces.[120] Therefore, the application of JMs in this field needs further improvement.

Recently, Yin et al.[121] reported a hybrid wettability Janus membrane with micropatterns for efficient fog collection, integrating within one-step laser-processed superhydrophobic patterns on a pristine hydrophilic copper sheet. During their work, it was demonstrated that the Janus membrane had high performance to apply in fog collection. They had a homemade fog-harvesting apparatus, which was established to evaluate the fog collection efficiency of different samples in Fig. 13c. A comparison of the as-prepared Janus sample with four samples, including the hydrophobic copper mesh, hydrophilic copper sheet, hydrophobic–hydrophilic copper mesh-sheet and as-treated copper mesh (superhydrophobic), showed that it had the highest efficiency of water collection. In order to achieve the optimal result, it is also necessary to satisfy both conditions: the
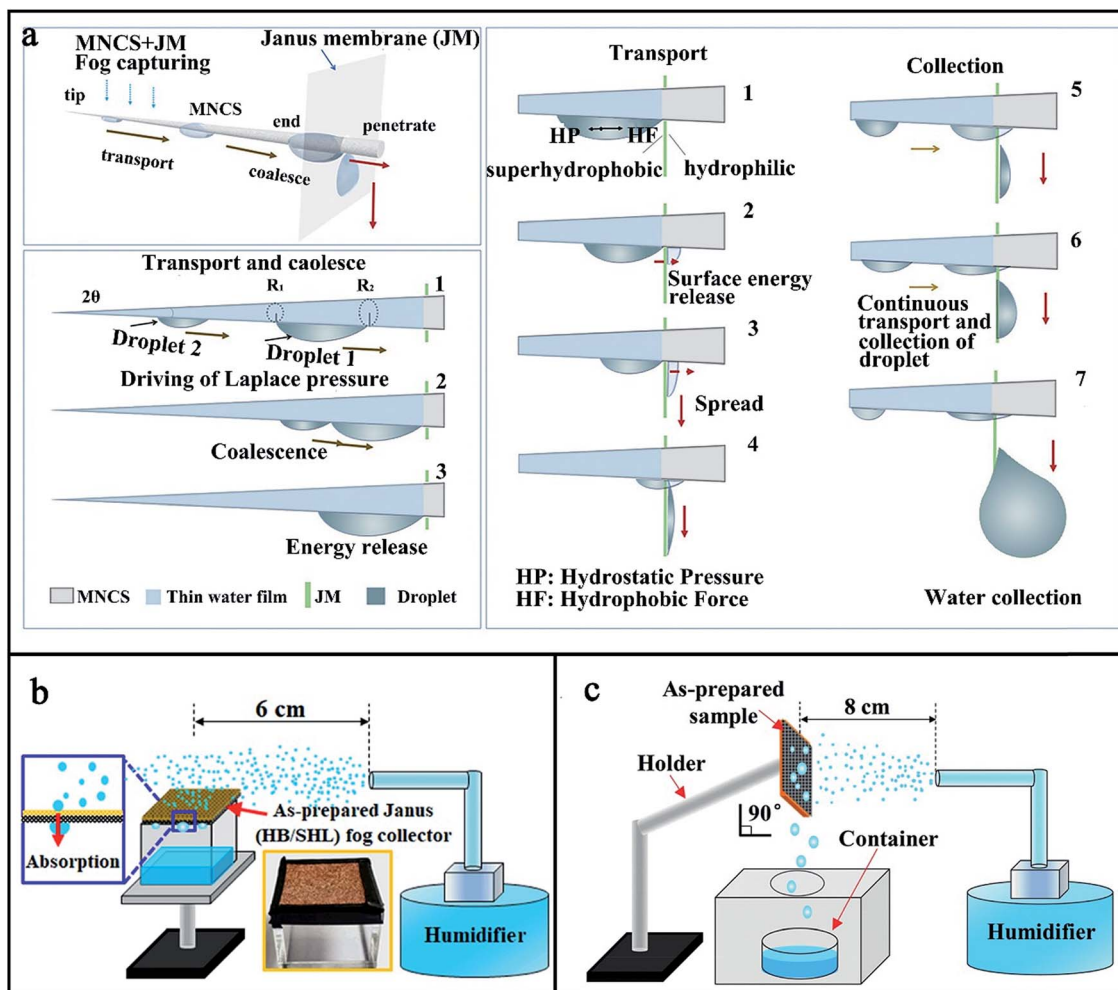
12938 | J. Mater. Chem. A, 2019, **7**, 12921–12950

This journal is © The Royal Society of Chemistry 2019

Fig. 13 (a) Illustration of fog collection. An overview of the whole fog harvesting process of the MNCS + JM, including capture, transport, coalescence, penetration, and collection. Adapted with permission.[122] Copyright 2018, Wiley–VCH. (b) Schematic of the purpose–built fog-collecting system. Adapted with permission.[58] Copyright 2018, American Chemical Society. (c) Schematic illustration of the homemade fog-harvesting system. Adapted with permission.[121] Copyright 2017, Royal Society of Chemistry.

adsorption of tiny water droplets and the removal of layer droplets. Fortunately, the as-prepared Janus membrane could simultaneously satisfy the two main factors. The fog collection process on the as-prepared membrane had also been explored. When the tiny water droplets came into contact with the copper sheet, they were trapped on it. Gradually, the droplets grew and detached from the surface of the as-prepared membrane. Although this method improved the fog-collecting efficiency, it was also restricted by the homemade fog-harvesting system, which was placed vertically and the water droplets were driven only by gravity. Furthermore, this water harvesting technology also suffered from problems since the harvesting process was complex and time-consuming. Therefore, further improvement needs to be made to construct novel Janus membranes, which not only have a low fabrication cost and simple fabrication process, but also exhibit high fog-collection efficiency. Therein, a Janus copper foam with nanoparticles on one side was prepared *via* one-step femtosecond laser direct writing technology,[58] which could overcome the above-mentioned

problems. Compared to other membranes, the as-prepared Janus foam showed excellent water collection efficiency, which could accelerate the penetration of water droplets from the hydrophobic side to superhydrophilic side due to the property of unidirectional liquid transportation. A fog collecting device consisting of the laser-structured Janus foam, with the super-hydrophilic side directed toward a transparent vessel and the hydrophobic side directed toward the air, exhibited excellent fog collection ability, as demonstrated in Fig. 13b. The fog collection devices mentioned above use only the Janus membrane, whereas some collection devices of the Janus membrane combined with other devices have also appeared, which can display more higher collection efficiency. For example, a micro/nanostructured conical spine and Janus membrane integrative system (MNCS + JM) was designed in order to collect tiny fog droplets (see Fig. 13a).[122] This system functions based on a wettability-integrated strategy in which water droplets were collected *via* a series of processes: droplet capture, transport, coalescence and penetration. The collected

water droplets spread on the hydrophilic surface of the Janus membrane for water collection. It can be observed that the formation and transport of water droplets in a short time reveal a prominent droplet transport efficiency of fog harvesting. For such a MNCS + JM system, both relative humidity and the effective length of spine are important for high efficiency water collection. In addition, the numbers of spines also affect the water collection rate. Therefore, a conclusion can be drawn that a higher water collection rate can be realized by adjusting relative humidity, the effective length of MNCS, and the extent of the hydrophilic surface. In short, the design of JMs is crucial for fog-collection, which can be applied to provide a sustainable water solution for arid regions with freshwater scarcity and further facilitate our lives. In addition, our group's research on the direction of fog harvesting has also matured. Zhong *et al.*[123] prepared a hydrophilic–hydrophobic/hydrophilic Janus copper mesh that not only has low-cost, but also has a high efficiency of fog harvesting. It should be noted that this Janus copper mesh cooperates various harvesting mechanisms together, showing ~800% enhancement in fog harvesting.

4.2 Oil–water separation

JMs can be applied in many aspects, especially in oil–water separation due to the opposite wettability on each surface. However, ordinary hydrophobic/hydrophilic membranes are not suitable for oil–water separation because both oil and water can infiltrate them. Fortunately, the function of the Janus membrane can be improved by adjusting the through-thickness of hydrophobic/hydrophilic layers.[124,125] It is important to realize unidirectional liquid transportation by adjusting the thickness of each layer. If the hydrophilic layer is thinner than the hydrophobic layer, the unidirectional penetration of oil droplets can be realized.[126–128] In contrast, when the hydrophobic layer is thinner than the hydrophilic layer, it will facilitate unidirectional penetration of water droplets.[129] For filtration separation of hydrophobic/hydrophilic JMs, the first separation type is using the water repellent property of the Janus membrane, which has a thick hydrophobic layer to achieve the "oil-removing" process. And the other separation type is the "water-removing" way, which can be realized on the Janus membrane with a thin hydrophobic layer (see Fig. 14). Moreover, it is convenient for separating oil in the oil–water mixture by underwater superoleophobic/underwater superoleophilic (solid surfaces with a static oil contact angle close to 0°) JMs.
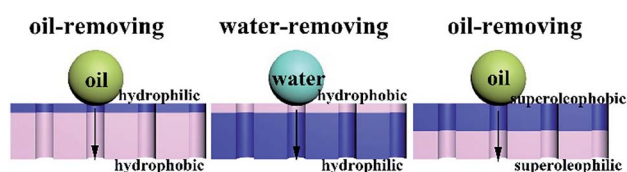

Fig. 14 Schematic of three separating types of Janus membranes: the thin hydrophilic layer to achieve the "oil-removing" process, the thin hydrophobic layer to realize the "water-removing" process, and the superoleophobic/superoleophilic Janus membrane to realize the "oil-removing" process.

For the former hydrophobic/hydrophilic membrane, this type of oil–water separation has been widely studied in the laboratory. For example, a novel oil-unidirectional Janus membrane possessed unidirectional oil transport properties because of its particular structure of the relatively thick hydrophobic layer and thin hydrophilic layer.[126] The Janus membrane was applied to integrated capture and lossless transportation of oil droplets and it could also effectively draw micrometer-sized oil from the oil-in-water emulsion. When the Janus membrane was placed at the oil–water interface with the hydrophilic layer toward oil, an oil droplet easily penetrated through the hydrophilic layer and reached the hydrophobic layer by the aid of the high resulting Laplace pressure. In contrast, when the Janus membrane was placed in the opposite direction, the oil droplet would immediately spread out on the hydrophobic layer. The oil droplet with the curved interface created a larger Laplace pressure while the contrary fixed mode exhibited negligible Laplace pressure. Therefore, there was no enough pressure to push the spread oil through the hydrophobic layer, resulting in the blockage of oil. In addition, there was a homemade collector, a mini Janus boat, which was folded by the Janus membrane and utilized to trap the oil droplets, as shown in Fig. 15a. Compared with the non-Janus hydrophobic collector, the Janus collector could not only highly efficiently collect oil spills but also tightly lock the collected oil even when they were lifted up into the air. In addition, JM-O could realize recovery after the use in oil-in-water emulsion separation. It is noted that the hydrophilic layer of the "oil-diode" Janus membrane (JM-O) needs to be pre-wetted by water and the hydrophobic layer of JM-O is pre-wetted by oils. Besides, the unique property of diode-like unidirectional oil transportation enabled the Janus membrane to effectively draw micro-sized oil droplets in oil-in-water emulsion and realize oil purification from the emulsion.

Another Janus membrane *via* grafting poly (*N,N*-dimethylaminoethyl methacrylate) (PDMAEMA) and poly(dimethylsiloxane) (PDMS) onto the two opposite sides of a cotton fabric was prepared by Wang and colleagues.[127] This Janus membrane included a PDMS superhydrophobic layer, whereas the other side was a hydrophilic layer. It was meaningful for the Janus membrane to be applied to separate oil from oil-in-water emulsion. The most interesting thing was that only when the hydrophilic side faced the feed emulsion, it could separate oil from oil-in-water emulsions (Fig. 15b). In contrast, when the hydrophobic side was exposed to the emulsion, no liquid permeated the membrane. Another definitive work was also presented by Wang and co-workers.[125] On this basis, they utilized an asymmetric environment to synthesize an *in situ*-generated Janus membrane again *via* a stimuli-responsive coating from a single polymer. Interestingly, these two different Janus membranes have the same oil separation principle. In their work, two halves of an H-shaped cell were divided by a Janus membrane. With powerful stirring, the emulsion knocked the membrane and demulsification and separation started. During this process, when the emulsion attached on the hydrophilic surface, water could only wet the surface without penetrating through the membrane due to the protection by the superhydrophobic layer. The hydrostatic pressure exerted on
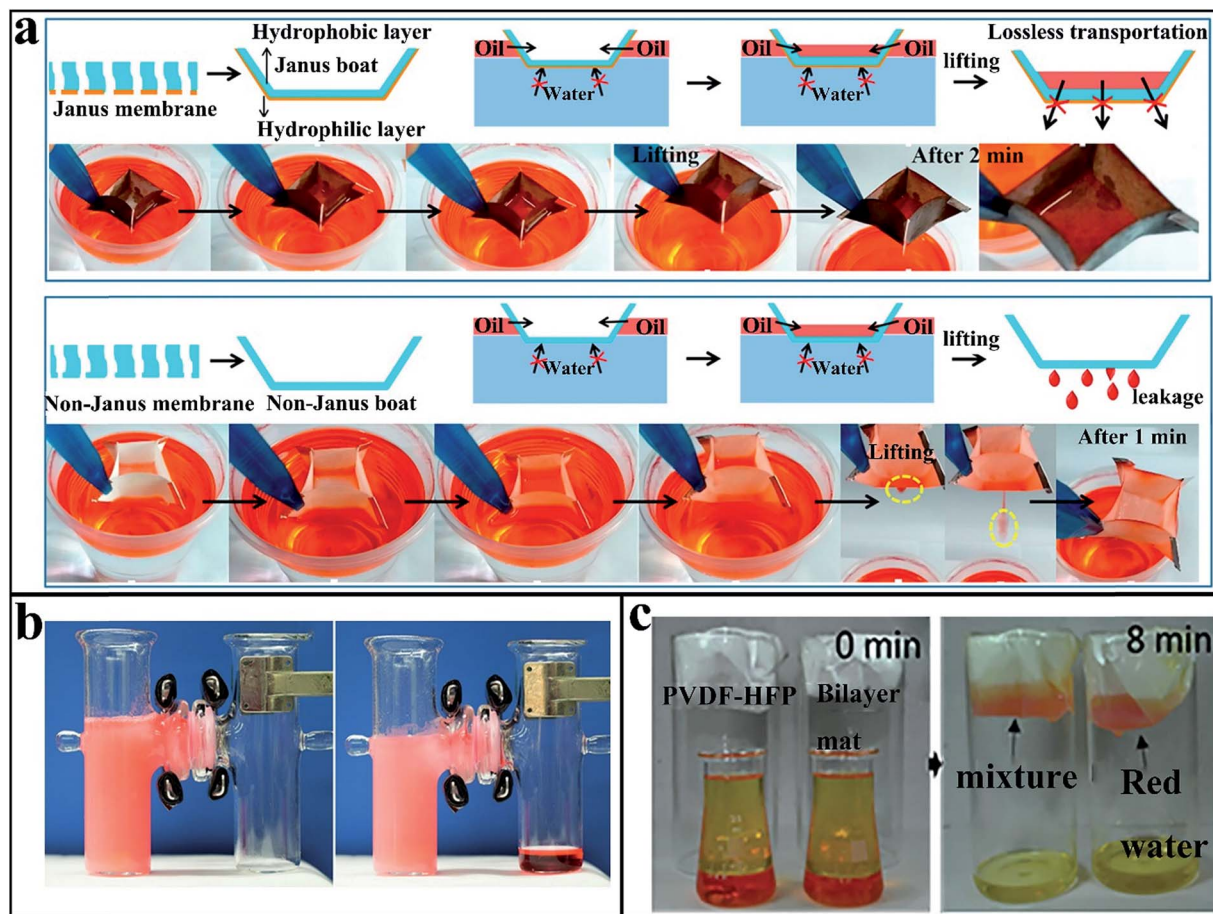
12940 | *J. Mater. Chem. A*, 2019, **7**, 12921–12950

This journal is © The Royal Society of Chemistry 2019

Fig. 15 (a) A Janus collector (a thin hydrophilic layer as an external surface) fabricated using JM-O showing efficient collection and lossless transportation of oil spills, while the collected oil leaks out from a common homogeneous hydrophobic collector after lifting. Adapted with permission.[126] Copyright 2018, Elsevier B. V. (b) Photographs showing the status of a separation experiment at time $t = 0$ s (on the left) and $t = 300$ s (on the right). Adapted with permission.[127] Copyright 2016, Wiley-VCH. (c) Photos taken during separation of diesel from water using nanofibrous membranes. During the test, the liquid was poured gently onto the fibrous membrane. Reproduced with permission.[62] Copyright 2015, Wiley-VCH.

the membrane by the column of the emulsion in the burette accelerated the separation. Meanwhile, owing to the oil filling of the superhydrophobic pores, water permeation can be prevented and oil transport can be facilitated. In conclusion, these prepared JMs functioned as filters to separate oil from various simple oil–water mixtures as well as oil-in-water emulsions. The oil separation flux was high and the separation was efficient.

After that, An *et al.*[128] also fabricated a Janus membrane which realized oil deemulsification and oil–water separation based on the unidirectional transport of oil and water. Owing to the charge-screening effect, the Janus membrane not only could effectively separate heavy oil from oil-in-water emulsions but also could separate light oil through deemulsification. The hydrophilic layer destabilized the emulsion by electrostatic interactions and facilitated the coalescence of oil drops. According to the deemulsification function of the hydrophilic layers, the pores of the hydrophobic layer could be filled with the coalesced oil and then the coalesced oil selectively permeated through the membrane, leading to effective oil separation. For a homemade device with a coated Janus membrane, the

Janus membrane was vertically contacted with the oil-in-water emulsion. The hydrophilic side was exposed to the emulsion and a clear and transparent filtrate without any water droplets was obtained on the other side. During this process, the hydrophobic layer adequately absorbed the demulsified oil, which could permeate through the Janus membrane spontaneously. Meanwhile, water cannot permeate into the pores of the Janus membrane due to the low solubility in the oil phase. In principle, when the transmembrane pressure was high enough, oil permeation would start after deemulsification.

Besides the above mentioned separation, the other separation type called the "water-removing" way has also been studied.[124,129] A Janus membrane consisting of a thick hydrophilic layer and thin hydrophobic layer could easily implement the "water-removing" way to separate the oil–water mixture.[129] Due to the special selectivity and unidirectional liquid permeability of this Janus membrane, unidirectional transport of water droplets can be achieved when the hydrophobic side orients toward oil.

Wang *et al.*[62] reported an underwater superoleophobic/oleophilic Janus membrane with unidirectional oil transport properties. Most interestingly, this Janus membrane was highly superhydrophobic on both sides, whereas it allowed unidirectional oil transport just from the underwater superoleophobic side to the oleophilic side. As is well known, the highly water-repellent and unidirectional oil transport ability of the Janus membrane would have strong water-rejection and oil-transport efficiency in oil–water separation. As demonstrated in Fig. 15c, oil–water separation on this Janus membrane was faster than that on the single-layer oleophilic membrane because the underwater oleophobic side created a larger Laplace pressure of oil thus accelerating the penetration of oil through the membrane.

4.3 Membrane distillation

Membrane distillation is a thermally driven process for desalination and sewage treatment, and has attracted great attention in recent years due to its advantages.[130] Such JMs have also become promising candidates for membrane distillation. During the membrane distillation process, it is important for the membrane to possess high mass transfer and low heat transfer to enhance the permeation flux and maintain the driving force arising from different temperatures. Traditional membranes used in membrane distillation need hydrophobic properties and high entry pressure to maintain vapor-filled pores. For conventional hydrophobic membranes, the heat and mass transfer will increase simultaneously when the thickness of the membrane increases, leading to a challenge for direct contact membrane distillation.

Therefore, the thickness of the hydrophobic layer is quite important in the membrane distillation process and it plays a crucial role in ensuring superior permeation flux because of the permeation resistance. Low heat transfer and high mass transfer are conducive to improving the vapor permeation flux,

so that it is suitable to reduce the vapor transport distance *via* a thin hydrophobic layer and achieve high permeability, while ensuring the overall membrane thickness *via* a thick hydrophilic layer to cut down heat loss, and the specific process is shown in Fig. 16a.[131,132] It is worth mentioning that the Janus membrane with asymmetric wettability has the ideal characteristic for overcoming the trade-off relationship between flux and conductive heat loss and it can also be applied to improve the contradictory requirements in membrane distillation. In recent years, researchers developed a series of hydrophobic/hydrophilic JMs to reduce the permeation resistance and meet the requirement of heat resistance in membrane distillation. For example, Yang *et al.*[131] prepared a Janus hollow membrane with high salt rejection and nice long-term stability, and also analyzed the mass and heat transfer in the Janus membrane during the direct contact membrane distillation process. During the direct contact membrane distillation test process, the Janus membrane exhibited an improved permeate flux with increasing deposition time and operation temperature, and the flux improvement was up to 120% for the Janus membrane deposited for 6 h with 80 °C feed. Furthermore, the Janus membrane with 4 h deposition showed excellent performance in both average permeate flux (above 6 L m^{-2} h^{-1}) and rejection (above 99%) over 72 h continuous operation.

In addition, the most typical membrane distillation membranes were made of common hydrophobic materials, which could primely work with relatively "clean" feed waters but fail for challenging feed waters, such as wastewater.[133,134] There exist a small number of membranes so far that can simultaneously resist wetting and fouling. Luckily, a pristine Janus membrane with special wetting properties had been developed to solve the problems of fouling and wetting in membrane distillation. Huang and co-workers prepared a Janus membrane consisting of an omniphobic substrate and an in-air hydrophilic, underwater superoleophobic layer was applied in
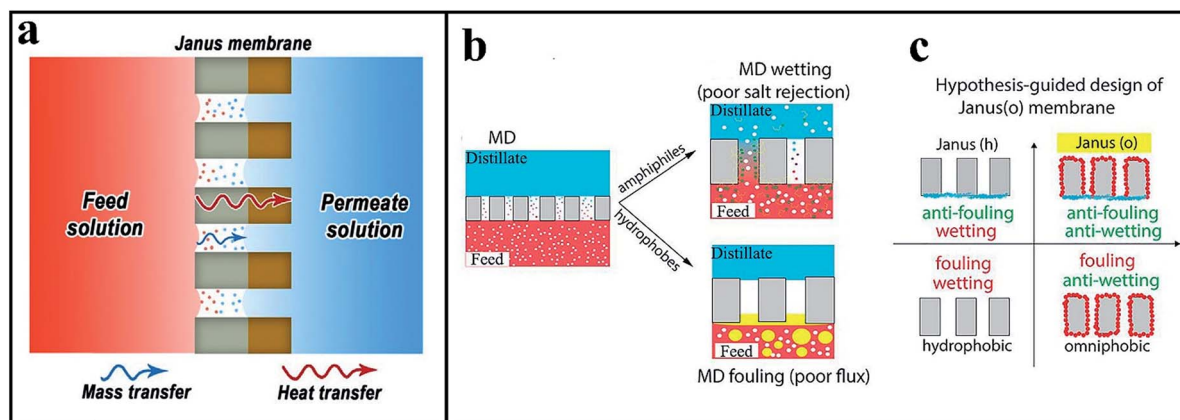

Fig. 16 (a) Schematic picture of the mass and heat transfer in a Janus membrane during the direct contact membrane distillation process. Adapted with permission.[131] Copyright 2017, Elsevier B. V. (b-left) Working mechanism of a membrane distillation process, and the white dots represent salts, which are rejected by the membrane. (b-right) Illustration of surfactant-induced wetting in a membrane distillation process and oil fouling in a membrane distillation process. (c) Illustration of the hypothesis that only a Janus membrane with an omniphobic substrate (*i.e.*, a Janus(o) membrane) can achieve simultaneous fouling and wetting resistance. Reproduced with permission.[135] Copyright 2017, American Chemical Society.

12942 | *J. Mater. Chem. A*, 2019, **7**, 12921–12950

This journal is © The Royal Society of Chemistry 2019

membrane distillation, which could simultaneously overcome the problems of fouling and wetting in membrane distillation.[135] Compared with the reference membranes, including the hydrophobic PVDF-HFP membrane, the omniphobic membrane and the hydrophobic/hydrophilic membrane, the as-prepared Janus membrane showed excellent and stable performance both in water flux and salt rejection, as demonstrated in Fig. 16. After the wetting experiments, the hydrophobic membrane was wetted easily, but the as-prepared Janus membrane was still able to sustain waterless (see Fig. 16c). For membrane distillation fouling experiments, the hydrophobic membrane was severely fouled with oil stains on the surface and it could not be reversible, but only minimal oil foulants stuck on the as-prepared Janus membrane surface after rinsing with deionized water (shown in Fig. 16c). Therefore, this Janus membrane can potentially transform membrane distillation into a viable technology for desalinating hypersaline wastewater with complex compositions using low-grade-thermal energy.

The distinctive advantage of the dual-layer Janus membrane for membrane distillation application is easily justified. Under a suitable range of membrane thicknesses, there would be a maximum permeation flux. However, it is necessary to tackle the challenges of delamination between the two polymer layers and dense interface morphology. The former would result in a defective membrane, while the latter could significantly increase the substructure resistance for vapor transport. Fortunately, there are lots of methods to solve these problems resulting in high flux and enhanced mechanical properties for membrane distillation. For example, Liu and colleagues[136] prepared a dual-layer Janus membrane, which consisted of a hydrophobic layer with an optimal range of 30–60 μm and a relatively thick hydrophilic layer. Compared to other membranes reported in the literature, the as-prepared Janus membrane indicated the highest flux thus far under various temperature conditions due to a unique asymmetric hydrophobic/hydrophilic structure. The water vapor transports through the hydrophobic layer of the Janus membrane which is vapor-filled space and condenses at the hydrophobic/hydrophilic interface. However, there is still a lack of studies and understanding on the integration mechanism of hydrophobic and hydrophilic layers and how it will affect membrane distillation performance. Recently, Qtaishat et al.[137] proposed a vapor transport mechanism and temperature profiles, which could explain the decreasing trend of flux. All in all, Janus membranes have great potential in membrane distillation applications as they can achieve a very thin hydrophobic layer and thus high permeability, while the addition of a thick hydrophilic layer can maintain the mechanical strength and potentially reduce the conductive heat loss through the membrane.[132,138]

4.4 Sensors

Another important application of JMs lies in sensing humidity stress of a humid environment, as revealed by Tian et al. in our group.[139] It was found that water-induced deformation could occur in the Janus paper because of the asymmetric wettability and hygroscopicity. Additionally, special Janus paper was highly desirable for environment electric sensors and electric relays, as the Janus paper achieved the conversion from deformation signals to the desirable electric signals. Furthermore, multi-walled carbon nanotubes (MWCNTs) were put into the hydrophobic region to construct a conductive network to satisfy the requirement, namely, the Janus paper could realize the conversion from variation of stress to electric signals. When the Janus paper was placed in a humid environment, water droplets would migrate into both the surfaces of the Janus paper, leading to surfaces of differential water concentration, and thus, the hydrophilic region became swollen while the other side became shrunken, because the water droplets well repelled on the hydrophobic side but could spread and permeate into the hydrophilic side.

Therefore, it is preferred to design materials with Janus features, and thus partial gathering of water droplets and directional deformation can be realized. The resistance of the polymer/MWCNT conductive network resulted from the Janus paper that deformed in a humid environment. During the experiment, the humidification capacity and relative humidity were transformed into deformation signals, and further converted into electric signals. In a gaseous humid atmosphere, unsaturated deformation would exist until a balance between hygroscopicity and volatilization is achieved. Another important test was that observing the stability of the Janus paper. A conclusion could be drawn that, after cycling, the Janus paper was highly stable in both condensed moisture airflow and gaseous humid atmosphere, and was appropriate to be applied as an environment electric sensor and electric relay.

Nevertheless, the actuation of current actuators is primarily triggered by a single stimulus at a slow rate of deformation because Janus materials only have one performance, the moisture-responsive performance or the thermal-responsive performance. However, a graphene-based Janus membrane was fabricated successfully by Zhang et al.,[140] which had both the performances. And this Janus membrane showed different actuations and possessed fast and reversible response properties. This as-prepared Janus membrane was composed of a graphene oxides (GO) layer and a reduced GO (RGO) layer, and exhibited a rapid response to humidity and temperature. It has been proven that the GO layer is rich in oxygen-containing functional groups, as well as being hydrophilic and elec-insulating. The obtained RGO layer created with HI-reduction showed hydrophobicity, thermal conductivity and electrical conductivity. It was interesting that the Janus membrane with the GO surface toward outside could crimp on the short-side when it was put in an environment with a humidity of 55%, which was attributed to the hygroscopic expansion of the GO layer, as shown in Fig. 17. Nevertheless, the GO/RGO Janus membrane would bend on the long-side and roll up in the opposite layer with the RGO surface toward outside at a temperature of 65 °C due to the thermal expansion of the RGO layer. The most interesting thing was that, owing to the favourable electrical conductivity of the RGO layer, the GO/RGO Janus membrane was applied to connect a circuit and switch
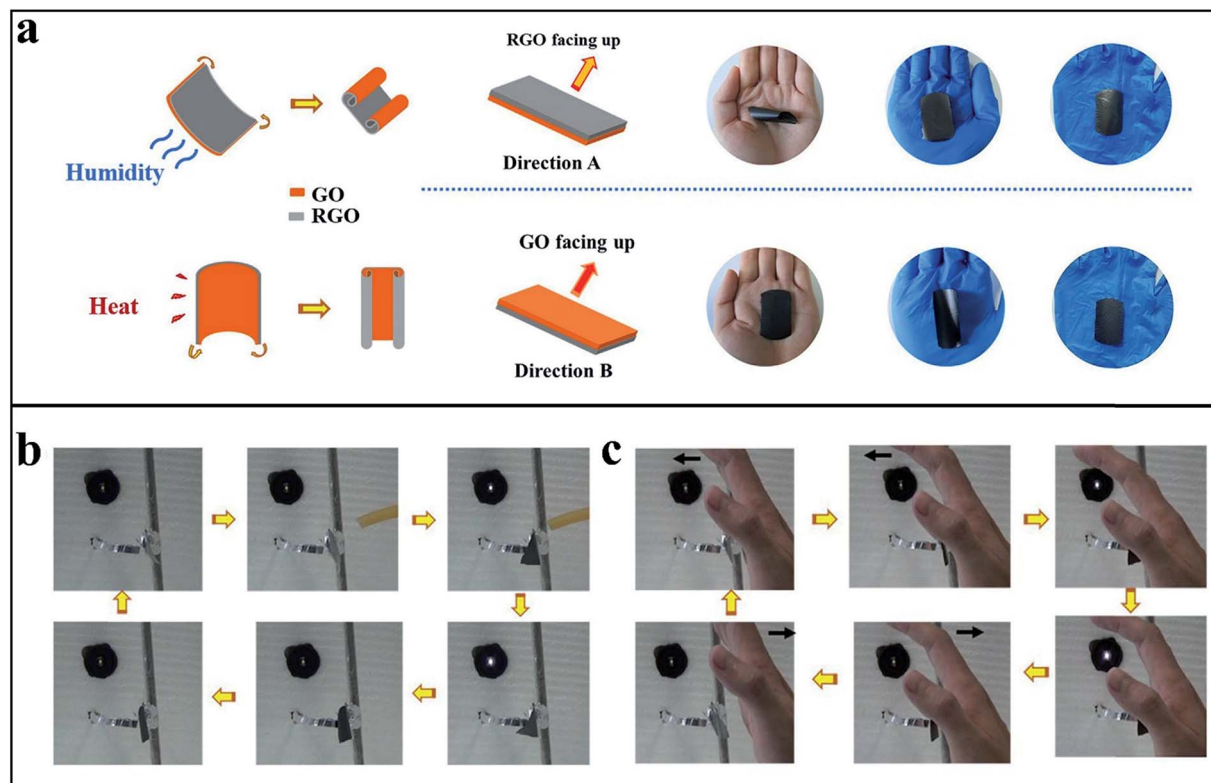
This journal is © The Royal Society of Chemistry 2019

J. Mater. Chem. A, 2019, 7, 12921–12950 | 12943

Fig. 17 (a) Schematic illustrations of the moisture/thermal responsive mechanism of the GO/RGO Janus membrane. (a-right) Schematic illustrations of the placement directions of the GO/RGO Janus film for the responsiveness testing. The smart perceptual switch triggered by (b) moist-air supply and (c) a sweaty hand. Reproduced with permission.[140] Copyright 2018, Elsevier B. V.

a bulb on/off, which was induced by the moist-air and a sweaty hand (see Fig. 17b and c).

Similar to this work, Cheng *et al.*[141] fabricated a one single graphene oxide (GO) membrane for responsive actuation, which had an asymmetric surface structure on its two surfaces. Owing to the peculiar structure, the GO membrane could turn into a responsive actuator to bend deformation along with changeable humidity and temperature. Interestingly, RGO circuits were prepared by exposing the smooth side of the GO film to a laser beam, and the deformation and output electrical signals could be detected in real time by using a CHI660D electrochemical workstation. During the test process, it was found that under infrared light, a remote thermal source, the GO membrane could bend to the rough side due to water desorption. In addition, the bending direction varied with humidity. When the RH exceeded 45% in the environment, the wrinkles on the rough surface were in a relaxation state by taking water molecules, resulting in the deformation on the smooth side, while the deformation would occur on the rough side under the opposite conditions. In a word, it was of special importance for the asymmetric responsiveness of the GO membrane to keep roughness difference on the surface. These outcomes would be of great significance in designing more efficient responsive actuation materials by combining both special surface chemistry and surface topographies.

Generally speaking, there are lots of advantages for some JMs with bilayer structures, which have diverse behaviors in response to external stimuli, including humidity, light and

electricity, but the main problem with bilayers actuators is that poor adhesion and even stratification may occur, leading to poor stability and repeatability. So, fabricating distinctive and stable actuators, which could respond to various stimuli and display an obvious curve, is extremely essential. Therein, an IrGO/rGO Janus membrane with strong adhesion and large deformation rate consisting of two asymmetric wettability layers, which was used to respond to multiple stimuli, did a good job of meeting these conditions.[142] Owing to the asymmetric wettability, the capabilities of absorption and desorption of water in this membrane were different, resulting in sensitive bending and deformation that could be applied as a humidity-driven or thermal-driven actuator. Sensing behavior, including the bending phenomenon, always takes place in air. It is worth mentioning that a polymeric Janus membrane with rapid and reversible folding resulting from inducement of organic solvents could happen both in air and in water, extending the range of applications, including artificial muscles and soft robotics.[59]

4.5 Applications of Janus membranes related to the unidirectional behavior of bubbles

Another interesting application of Janus membranes is bubble aeration. It should be noted that the unidirectional transportation of gas bubbles is necessary to overcome existing problems in industrial processes, including the corrosion of ocean vessels and fluid transportation in pipes and so on. Gas

12944 | *J. Mater. Chem. A*, 2019, **7**, 12921–12950

This journal is © The Royal Society of Chemistry 2019

bubbles are of great significance in practical applications, improving heat transfer in the ocean, promoting gas/liquid mass transfer and improving the flotation recovery of fine mineral particles.[143,144] In the practical applications of gas bubbles, there are many hidden dangers as well as benefits. For example, in the process of crude oil transportation, the oil–water mixture mixed with gas bubbles such as carbon dioxide and oxygen will corrode pipes leading to the waste of resources.[145,146] Traditional hydrophilic membranes are usually aerophobic underwater, which is conducive to the release of air bubbles from the membrane and generation of smaller bubbles, whereas there still exists a series of problems using these membranes to remove gas dissolved in liquid.[147,148] What is more, the property of aerophobicity underwater will increase the pressure of gas transportation, which requires more energy from the outside and leads to a large amount of energy consumption. Therefore, it is urgent to prepare specific materials to control the unidirectional transportation of air bubbles. Recently, JMs with the property of underwater unidirectional gas bubbles or air penetration were fabricated by researchers, which might be applied to practical applications to satisfy these problems. A Janus membrane consisting of the hydrophilic/underwater superaerophobic side and hydrophobic side was applied for gas absorption and purification.[56] Compared to hydrophobic membranes, this Janus membrane showed a special advantage, creating fine bubbles, which not only could preserve the immobilized enzyme, but also provided oxygen for many oxidation reactions.

Besides the aforementioned applications, JMs can also be applied in biocatalytic gas–liquid membrane reactors for CO_2 hydration and conversion. For the conventional gas–liquid reactor, the total mass transfer resistance increases with the wetting of the membrane surface, even if the pores of a very thin membrane are wetted slightly. Therefore, the hydrophobicity of membranes is often used to prevent membrane pore wetting. However, enzyme immobilization on hydrophobic membranes usually leads to denaturation caused by the interaction between the hydrophobic peptide chains and the surface. Considering these issues, the gas–liquid reactor should be further optimized through the following aspects: continuous liquid flow instead of recirculation to reduce the accumulated CO_2 in the liquid side; and membranes with lower mass transfer resistance.[149] The optimization method mentioned above is very well implemented. Especially, the last aspect can be realized with a Janus membrane. For the Janus membrane, there is a hydrophilic layer to achieve highly efficient enzyme immobilization and there is a hydrophobic layer to prevent membrane pore wetting, facilitating mass transfer. Yang et al.[150] developed a Janus membrane through a facile single-sided polydopamine deposition technique, by which the preparation of Janus biocatalytic membranes for CO_2 hydration can be potentially realized. The gas/liquid mass transfer mainly depends on the gas/liquid contact area and contact time and reducing the bubble size can improve standing time underwater, further leading to an enhancement in gas/liquid mass transfer. In addition, the performance of the reactor can also be improved by appropriate selection of membrane modules, which can promote the mass

transfer efficiency. Typically, biocatalytic TiO_2 nanoparticles with covalently immobilized carbonic anhydrase (CA) are suspended in the solvent absorbent, not only increasing the biocatalytic performance but highly improving the CO_2 hydration rate. It is worth noting that this bubbling reactor possesses nearly 20 times higher CO_2 hydration efficiency than the CO_2 hydration reactor they previously reported. In order to further promote the CO_2 hydration rate, CA should be fixed as close as possible to the gas–liquid interface to ensure proper contact with CO_2 and water. Compared with the experiment mentioned above, biocatalytic TiO_2 nanoparticles with covalently immobilized CA are suspended in the solution, and the CA effectively immobilized on the hydrophilic coating layer can improve the highly efficient reaction between CA, CO_2 and water. During the CO_2 hydration process, the hydrated CO_2 always needs a longer distance to pass through the membrane pores into the liquid so that partially hydrated CO_2 can react with CA on the hydrophilic layer, resulting in dehydration and reducing the CO_2 hydration rate. Hou et al.[151] integrated a Janus membrane with a hydrophilic CNT coating layer, where the CA is immobilized, and the other superhydrophobic side is the PVDF membrane support. In order to shorten the CO_2 diffusion distance and enhance the CO_2 hydration efficiency, through a large number of experiments, they determined the optimal membrane configuration and thickness and proved that the Janus membrane is a promising alternative for CO_2 capture from flue gas and can be used for enzymatic gas–liquid reactors. For another Janus reactor, there is a highly efficient enzymatic CO_2 nanocascade at the air–liquid interface, and nanocascades containing the nanoscale compartmentalized CA and formic dehydrogenase are placed at the gas–liquid interface, leading to a high substrate concentration gradient.[152] Once CO_2 diffuses into the hydrophilic layer and enters the liquid phase, it can immediately react with CA and convert to formic acid. The as-prepared Janus biocatalytic membrane has a 2.5 times higher CO_2 hydration rate compared with the original hydrophobic membrane when used in a gas–liquid membrane contactor, and it can be reused for eight cycles without losing its efficiency, and the schematic diagram of the gas liquid contactor is shown in Fig. 18a.

Underwater bubble manipulation by surface microstructures has also been a critical research area from natural biological to industrial processes. The application of the unidirectional behaviors of underwater bubbles in other fields has also been studied. A superhydrophobic/hydrophilic Janus aluminum membrane was fabricated, which has tapered micropore arrays, showing a distinctive unidirectional air bubble transport ability.[153] As we all know, once CO_2 is introduced into the purple litmus solution, there will be a magical phenomenon that the solution turns red. According to that, this Janus membrane has been shown to support an air-participating chemical/physical process during discoloration of purple litmus solution through the CO_2 injection process, which helps the air to participate in underwater applications. However, it should be noted that a large amount of research has focused on hydrophobic or hydrophilic materials and research about underwater bubble behavior has been relatively scarce. Therefore, controlling underwater bubble behavior on a solid surface and
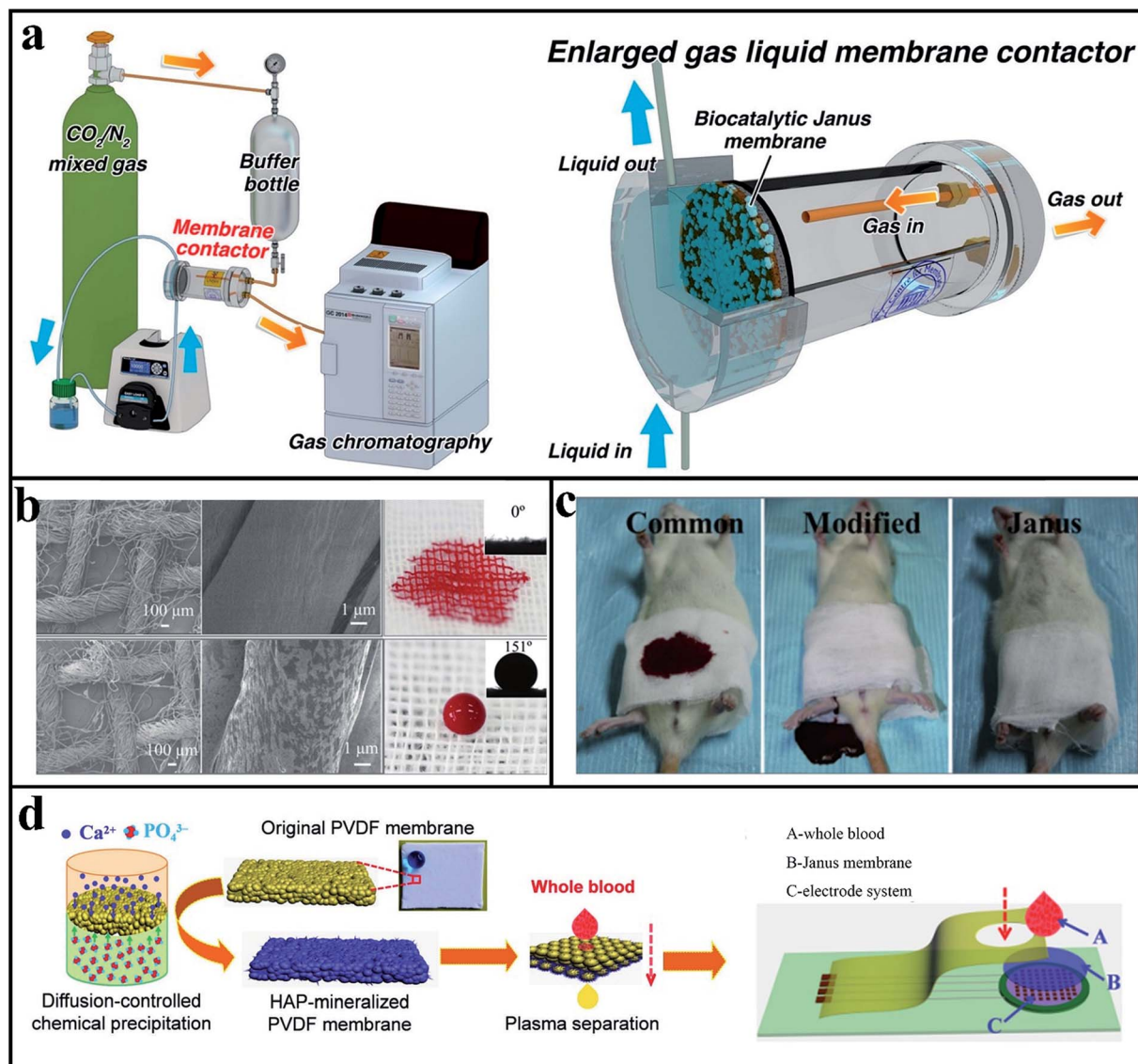
Fig. 18 (a) Schematic diagram of the gas liquid contactor. Adapted with permission.[152] Copyright 2017, American Chemical Society. (b) SEM images of the common and the modified gauze and digital photos showing blood on the common and the modified gauze, and inserts are the corresponding blood CA images. (c) Photos of the rats with the injured femoral artery wrapped with bilayer common gauze and Janus gauze, respectively. Adapted with permission.[155] Copyright 2018, Wiley-VCH. (d) Schematic of HAP mineralization of the porous superhydrophobic PVDF membranes through a diffusion-controlled chemical precipitation process for microliter quantities of plasma separation. (d-right) Schematic of a blood glucose monitor. A whole blood droplet permeates across the HAP-mineralized membrane to enter the enzyme (glucose oxidase) layer, wherein glucose concentration in the blood is detected. Reproduced with permission.[157] Copyright 2017, Royal Society of Chemistry.

fabricating artificial underwater superaerophobic, super-aerophilic surfaces or superaerophobic/superaerophilic Janus materials are great challenges so that a lot of research needs to be constantly done to overcome these problems and challenges.

4.6 Other applications

Besides the applications mentioned above, JMs also display endless potential in many other fields. JMs can also improve the performance of existing applications involving a hemostatic process, because they can meet the requirements of reducing blood loss and prolonging the survival time during a baseline emergency treatment. It is well known that the most used hemostatic material is cotton gauze with advantages of low cost, softness and breathability.[154] Nevertheless, there are still grand challenges such as unnecessary blood loss and serious damage that would occur due to the excessive blood absorbing by cotton gauze. Compared with hydrophobic gauzes and hydrophilic gauzes, Janus materials could overcome these problems: blood flowing away from the underneath of the gauze in the former case and the quick and complete absorbing of blood in the latter case. A Janus fabric was obtained by modifying only one surface with paraffin/hexane solution *via* a dip coating process

12946 | *J. Mater. Chem. A*, 2019, **7**, 12921–12950

This journal is © The Royal Society of Chemistry 2019

so that the modified layer was superhydrophobic where blood could not spread on, resulting from the low surface tension of paraffin and the surface roughness of the modified fabrics (see Fig. 18b).[155] As mentioned earlier, some JMs have been reported to have the property of unidirectional fluid transportation, where fluid could penetrate from the hydrophobic layer to the hydrophilic layer, whereas fluid would be blocked in the reverse direction. Owing to this particular property, effective bleeding control with reduced blood loss by more than 50% compared to common fabrics could be realized as well as the breathability was also largely maintained by using Janus fabrics because the pores were largely maintained after modification. Once the blood was dripping onto the hydrophilic layer, water in the blood could be absorbed immediately thus speeding up blood clotting, whereas the other side would prevent blood from wetting and permeating so that quick hemostasis and the decrease of blood loss could be achieved. As illustrated in Fig. 18c, a comparison of the Janus fabric with common gauze shows that the most important thing is that this improvement extended the survival time in the case of serious injury with a higher bleeding flow. Beyond these performance advantages, the Janus fabric also provided several additional benefits. Since the hydrophobic layer was dry and free of blood contamination, the bacteria had difficulty in contacting the wound, reducing the risk of wound infection as well as the transmission of infectious blood diseases.

Another potential application of the Janus membrane is the fast separation of a trace of blood. It is well known that red blood cells have a negative effect on glucose measurements, so it is necessary to develop a porous membrane to prevent red blood cells from entering the enzyme layer and reduce interference.[156] In order to achieve the goal of rapid separation of red blood cells, it is requisite for membranes to meet some conditions, including asymmetric wettability membranes with appropriate thickness to realize unidirectional liquid transportation and a pore size less than the diameter of the red blood cells to prevent them from passing through the membrane. Zhang et al.[157] composited an asymmetric Janus membrane by overlapping a hydrophilic layer with a hydrophobic layer to realize plasma separation and it was suitable for the separation of a small amount of blood to reduce symptoms for a patient, as shown in Fig. 18d. When a droplet of whole blood was dropped on the hydrophobic side of the Janus membrane, instead of spreading, the droplet could penetrate across the membrane from the hydrophobic layer to the hydrophilic layer to reduce the blood flow. The as-prepared Janus membrane was then installed together with the blood glucometer to measure the glucose level accurately. With improvement, the negative effect of hematocrit levels on the blood glucose measurements became smaller, and then an accurate and stable glucose current signal was detected due to less interference of red blood cells.

5   Conclusion and outlook

In this review, the development process of JMs has been introduced from the beginning. Next, recent advances in research on JMs have also been outlined, including some detailed preparation processes and the main properties. According to the prepared materials, we roughly classify JMs into three categories: polymeric Janus membranes, polymeric-inorganic Janus membranes and inorganic Janus membranes. The asymmetric wettability of the Janus membrane drives the unidirectional transportation of liquids and gas bubbles, which has attracted tremendous attention in recent years due to its potential applications. We have carried out detailed analysis and description of unidirectional transportation behaviors and discussed their systematic physical mechanisms. The asymmetric-wettability-dominated applications of oil–water separation, membrane distillation, fog-harvesting, sensors and others were then presented.

Although the creation of the Janus membrane provides a lot of convenience, there are still many problems that need to be overcome. Firstly, many materials are expensive and environmentally unfriendly, such as fluorine-containing materials, from the perspective of materials. Many commonly used preparation methods do not satisfy the qualitative and quantitative preparation of JMs, and even some methods cannot control the membrane thickness very well. There are still many problems with the currently prepared Janus membranes, including problems such as easy delamination, poor stability, and poor recyclability. In addition, preparation methods currently used cannot achieve large-scale production, and the prepared multifunctional JMs can only meet the applications of the laboratory and cannot realize industrial applications. Although a large amount of research has focused on the unidirectional transportation of liquids and gas bubbles, it is still impossible to accurately conduct specific force analysis and mechanism studies on transport behaviors in the cross-section direction of JMs. Most importantly, current research has always focused on the applications of asymmetric wettability and unidirectional transport behavior, limiting the versatile applications of JMs.

Janus membranes have great application prospects and will continue to receive attention. It is necessary to prepare a Janus membrane with good stability and strong mechanical properties by using economical, non-polluting and high-performance materials, which will be a future development trend. While retaining existing features, efforts are being made to introduce new features into the Janus membrane to expand its potential applications. In addition to the existing applications of the Janus membrane, sensors that respond to external stimuli still have great development prospects. Therefore, developing a new Janus membrane and applying it to other aspects is something that needs to be continued in the future.

Conflicts of interest

The authors declare no conflict of interest.

Acknowledgements

This journal is © The Royal Society of Chemistry 2019

J. Mater. Chem. A, 2019, **7**, 12921–12950 | **12947**

Notes and references

1 M. Gagarin, *The Oxford Encyclopedia of Ancient Greece and Rome*, Oxford University Press on Demand, 2010.

2 C. Casagrande, P. Fabre, E. Raphael and M. Veyssié, *Europhys. Lett.*, 1989, **9**, 251–255.

3 P. G. de Gennes, *Angew. Chem., Int. Ed.*, 1992, **31**, 842–845.

4 B. Wang, W. Liang, Z. Guo and W. Liu, *Chem. Soc. Rev.*, 2015, **44**, 336–361.

5 Y. S. Lee, B. K. Kaang, N. Han, H. J. Lee and W. San Choi, *J. Mater. Chem. A*, 2018, **6**, 16371–16381.

6 H. Han, S. Baik, B. Xu, J. Seo, S. Lee, S. Shin, J. Lee, J. Koo, Y. Mei, C. Pang and T. Lee, *Adv. Funct. Mater.*, 2017, **27**, 1701618.

7 C. Xu, R. Feng, F. Song, X. Wang and Y. Wang, *ACS Sustainable Chem. Eng.*, 2018, **6**, 14679–14684.

8 M. Agiorgousis, Y. Sun, D. West and S. Zhang, *ACS Appl. Energy Mater.*, 2018, **1**, 440–446.

9 P. Guo, C. Zeng, C. Wang and L. Zhang, *AIChE J.*, 2017, **63**, 4115–4123.

10 A. Walther and A. H. E. Müller, *Chem. Rev.*, 2013, **113**, 5194–5261.

11 L. Cheng, G. Zhang, L. Zhu, D. Chen and M. Jiang, *Angew. Chem., Int. Ed.*, 2008, **47**, 10171–10174.

12 J. Hu, S. Zhou, Y. Sun, X. Fang and L. Wu, *Chem. Soc. Rev.*, 2012, **41**, 4356–4378.

13 J. Yan, K. Chaudhary, S. Bae, J. Lewis and S. Granick, *Nat. Commun.*, 2013, **4**, 1516.

14 Y. Si, F. Yang and Z. Guo, *J. Colloid Interface Sci.*, 2016, **484**, 173–182.

15 P. Gibson, H. Schreuder-Gibson and D. Rivin, *Colloids Surf., A*, 2001, **187–188**, 469–481.

16 Y. Zhao, H. Wang, H. Zhou and T. Lin, *Small*, 2017, **13**, 1601070.

17 S. Ng, N. Noor and Z. Zheng, *NPG Asia Mater.*, 2018, **10**, 217–237.

18 Z. Zheng, C. Nottbohm, A. Turchanin, H. Muzik, A. Beyer, M. Heilemann, M. Sauer and A. Gölzhäuser, *Angew. Chem., Int. Ed.*, 2010, **49**, 8493–8497.

19 Z. Wang, Y. Li, S. Li, J. Guo and S. Zhang, *Chem. Commun.*, 2018, **54**, 10954–10957.

20 Q. Cheng, M. Li, Y. Zheng, B. Su, S. Wang and L. Jiang, *Soft Matter*, 2011, **7**, 5948–5951.

21 B. Yue, B. Zhang, J. You, Y. Li, L. Li and J. Li, *RSC Adv.*, 2016, **6**, 17215–17221.

22 E. A. Vogler, *Adv. Colloid Interface Sci.*, 1998, **74**, 69–117.

23 H. Yang, J. Hou, V. Chen and Z. Xu, *Angew. Chem., Int. Ed.*, 2016, **55**, 13398–13407.

24 Y. Shi, Y. Li, J. Wu, W. Wang, A. Dong and J. Zhang, *J. Biomater. Sci., Polym. Ed.*, 2014, **25**, 713–728.

25 Q. Wang, Y. Geng, J. Li, M. Yin, Y. Hu, Y. Liu and K. Pan, *Nanotechnology*, 2018, **29**, 135702.

26 J. Zhang, Y. Yang, Z. Zhang, P. Wang and X. Wang, *Adv. Mater.*, 2014, **26**, 1071–1075.

27 C. Zeng, H. Wang, H. Zhou and T. Lin, *RSC Adv.*, 2015, **5**, 61044–61050.

28 Y. Zhang and M. Barboiu, *Chem. Commun.*, 2015, **51**, 15925–15927.

29 J. Hou, C. Ji, G. Dong, B. Xiao, Y. Ye and V. Chen, *J. Mater. Chem. A*, 2015, **3**, 17032–17041.

30 J. Gu, P. Xiao, J. Chen, J. Zhang, Y. Huang and T. Chen, *ACS Appl. Mater. Interfaces*, 2014, **6**, 16204–16209.

31 J. Bai, Z. Shi, J. Yin, M. Tian and R. Qu, *Adv. Funct. Mater.*, 2018, **28**, 1800939.

32 J. Osicka, M. Ilčiková, A. Popelka, J. Filip, T. Bertok, J. Tkac and P. Kasak, *Langmuir*, 2016, **32**, 5491–5499.

33 X. Du, J. Li, A. Welle, L. Li, W. Feng and P. Levkin, *Adv. Mater.*, 2015, **27**, 4997–5001.

34 B. L. de Groot and H. Grubmüller, *Science*, 2001, **294**, 2353–2357.

35 J. Li, Y. Hou, Y. Liu, C. Hao, M. Li, M. Chaudhury, S. Yao and Z. Wang, *Nat. Phys.*, 2016, **12**, 606.

36 H. Li, M. Cao, X. Ma, Y. Zhang, X. Jin, K. Liu and L. Jiang, *Adv. Mater. Interfaces*, 2016, **3**, 1600276.

37 Y. Cui, D. Li and H. Bai, *Ind. Eng. Chem. Res.*, 2017, **56**, 4887–4897.

38 H. Geng, H. Bai, Y. Fan, S. Wang, T. Ba, C. Yu, M. Cao and L. Jiang, *Mater. Horiz.*, 2018, **5**, 303–308.

39 H. Zhou, H. Wang, H. Niu, C. Zeng, Y. Zhao, Z. Xu, S. Fu and T. Lin, *Adv. Mater. Interfaces*, 2016, **3**, 1600283.

40 M. Cao, K. Li, Z. Dong, C. Yu, S. Yang, C. Song, K. Liu and L. Jiang, *Adv. Funct. Mater.*, 2015, **25**, 4114–4119.

41 K. Yin, S. Yang, X. Dong, D. Chu, J. Duan and J. He, *Appl. Phys. Lett.*, 2018, **112**, 243701.

42 J. Yong, F. Chen, Y. Fang, J. Huo, Q. Yang, J. Zhang, H. Bian and X. Hou, *ACS Appl. Mater. Interfaces*, 2017, **9**, 39863–39871.

43 Z. Wang, X. Yang, Z. Cheng, Y. Liu, L. Shao and L. Jiang, *Mater. Horiz.*, 2017, **4**, 701–708.

44 Y. Zhang, M. Cao, Y. Peng, X. Jin, D. Tian, K. Liu and L. Jiang, *Adv. Funct. Mater.*, 2018, **28**, 1704220.

45 D. Miao, Z. Huang, X. Wang, J. Yu and B. Ding, *Small*, 2018, **14**, 1801527.

46 X. Pang, C. Wan, M. Wang and Z. Lin, *Angew. Chem., Int. Ed.*, 2014, **53**, 5524–5538.

47 B. Su, Y. Tian and L. Jiang, *J. Am. Chem. Soc.*, 2016, **138**, 1727–1748.

48 L. Wen, Y. Tian and L. Jiang, *Angew. Chem., Int. Ed.*, 2015, **54**, 3387–3399.

49 J. Yong, Q. Yang, F. Chen, D. Zhang, H. Bian, H. Ou, J. Si, G. Du and X. Hou, *Appl. Phys. A*, 2013, **111**, 243–249.

50 Y. Geng, P. Zhang, Q. Wang, Y. Liu and K. Pan, *J. Mater. Chem. B*, 2017, **5**, 5390–5396.

51 Z. Zhu, Z. Liu, L. Zhong, C. Song, W. Shi, F. Cui and W. Wang, *J. Membr. Sci.*, 2018, **563**, 602–609.

52 J. Yang, G. Wen, X. Gou, H. Song and Z. Guo, *J. Membr. Sci.*, 2018, **563**, 326–335.

53 Z. Cheng, B. Wang, H. Lai, P. Liu, D. Zhang, D. Tian, H. Liu, X. Yu, B. Sun and K. Sun, *Chem.–Asian J.*, 2017, **12**, 2085–2092.

54 Y. Zhao, C. Yu, H. Lan, M. Cao and L. Jiang, *Adv. Funct. Mater.*, 2017, **27**, 1701466.

55 Y. Si, L. Chen, F. Yang, F. Guo and Z. Guo, *J. Colloid Interface Sci.*, 2018, **509**, 346–352.

56 H. Yang, J. Hou, L. Wan, V. Chen and Z. Xu, *Adv. Mater. Interfaces*, 2016, **3**, 1500774.

57 D. Han, P. Xiao, J. Gu, J. Chen, Z. Cai, J. Zhang, W. Wang and T. Chen, *RSC Adv.*, 2014, **4**, 22759–22762.

58 K. Yin, S. Yang, X. Dong, D. Chu, J. Duan and J. He, *ACS Appl. Mater. Interfaces*, 2018, **10**, 31433–31440.

59 Q. Fu, H. Zhang, Z. Wang and M. Chiao, *J. Mater. Chem. B*, 2017, **5**, 4025–4030.

60 M. Wu, H. Yang, J. Wang, G. Wu and Z. Xu, *ACS Appl. Mater. Interfaces*, 2017, **9**, 5062–5066.

61 T. Li, F. Liu, S. Zhang, H. Lin, J. Wang and C. Y. Tang, *ACS Appl. Mater. Interfaces*, 2018, **10**, 24947–24954.

62 H. Wang, H. Zhou, H. Niu, J. Zhang, Y. Du and T. Lin, *Adv. Mater. Interfaces*, 2015, **2**, 1400506.

63 H. Wang, H. Zhou, W. Yang, Y. Zhao, J. Fang and T. Lin, *ACS Appl. Mater. Interfaces*, 2015, **7**, 22874–22880.

64 S. Yang, K. Yin, D. Chu, J. He and J. Duan, *Appl. Phys. Lett.*, 2018, **113**, 203701.

65 M. Fingas, *Handbook of Oil Spill Science and Technology*, John Wiley & Sons, Hoboken, New Jersey, 2014.

66 B. Bhushan and M. Nosonovsky, *Philos. Trans. R. Soc., A*, 2010, **368**, 4713–4728.

67 R. N. Wenzel, *Ind. Eng. Chem.*, 1936, **28**, 988–994.

68 Y. Tian and L. Jiang, *Nat. Mater.*, 2013, **12**, 291.

69 A. B. D. Cassie and S. Baxter, *Trans. Faraday Soc.*, 1944, **40**, 546–551.

70 Y. Si and Z. Guo, *Nanoscale*, 2015, **7**, 5922–5946.

71 M. Nosonovsky and B. Bhushan, *Multiscale Dissipative Mechanisms and Hierarchical Surfaces: Friction, Superhydrophobicity, and Biomimetics*, Springer Science & Business Media, 2008.

72 P. Gupta and B. Kandasubramanian, *ACS Appl. Mater. Interfaces*, 2017, **9**, 19102–19113.

73 P. Gore and B. Kandasubramanian, *J. Mater. Chem. A*, 2018, **6**, 7457–7479.

74 H. Zheng, Y. Zhang, Z. Peng and Y. Zhang, *J. Appl. Polym. Sci.*, 2004, **92**, 638–646.

75 K. Meera, R. Sankar, A. Murali, S. Jaisankar and A. Mandal, *Colloids Surf., B*, 2012, **90**, 204–210.

76 A. Giacomello, S. Meloni, M. Chinappi and M. Casciola, *Langmuir*, 2012, **28**, 10764–10772.

77 E. Savoy and F. Escobedo, *Langmuir*, 2012, **28**, 16080–16090.

78 W. Ren, *Langmuir*, 2014, **30**, 2879–2885.

79 X. Jing and Z. Guo, *J. Mater. Chem. A*, 2018, **6**, 16731–16768.

80 S. Li, S. Lamant, J. L. Carlier, M. Toubal, P. Campistron, X. Xu, G. Vereecke, V. Senez, V. Thomy and B. Nongaillard, *Langmuir*, 2014, **30**, 7601–7608.

81 X. Xu, G. Vereecke, C. Chen, G. Pourtois, S. Armini, N. Verellen, W. Tsai, D. Kim, E. Lee, C. Lin, P. Dorpe, H. Struyf, F. Holsteyns, V. Moshchalkov, J. Indekeu and S. D. Gendt, *ACS Nano*, 2014, **8**, 885–893.

82 V. Kondrashov and J. Rühe, *Langmuir*, 2014, **30**, 4342–4350.

83 K. K. Phani and S. K. Niyogi, *J. Am. Ceram. Soc.*, 1987, **70**, C-362–C-366.

84 Y. Zheng, X. Gao and L. Jiang, *Soft Matter*, 2007, **3**, 178–182.

85 Y. Zheng, H. Bai, Z. Huang, X. Tian, F. Nie, Y. Zhao, J. Zhai and L. Jiang, *Nature*, 2010, **463**, 640–643.

86 X. Tian, J. Li and X. Wang, *Soft Matter*, 2012, **8**, 2633–2637.

87 W. Hamilton III, J. Henschel and M. Seely, *S. Afr. J. Sci.*, 2003, **99**, 181.

88 H. Liu, J. Huang, F. Li, Z. Chen, K. Zhang, S. Al-Deyab and Y. Lai, *Cellulose*, 2017, **24**, 1129–1141.

89 J. Wu, N. Wang, L. Wang, H. Dong, Y. Zhao and L. Jiang, *Soft Matter*, 2012, **8**, 5996–5999.

90 H. Zhou, H. Wang, H. Niu and T. Lin, *Sci. Rep.*, 2013, **3**, 2964.

91 H. Cao, W. Gu, J. Fu, Y. Liu and S. Chen, *Appl. Surf. Sci.*, 2017, **412**, 599–605.

92 Y. Dong, J. Kong, S. Phua, C. Zhao, N. Thomas and X. Lu, *ACS Appl. Mater. Interfaces*, 2014, **6**, 14087–14095.

93 Y. Dong, J. Kong, C. Mu, C. Zhao, N. Thomas and X. Lu, *Mater. Des.*, 2015, **88**, 82–87.

94 N. Li, C. Yu, Y. Si, M. Song, Z. Dong and J. Lei, *ACS Appl. Mater. Interfaces*, 2018, **10**, 7504–7511.

95 K. Stephani and D. Goldstein, *J. Fluids Eng.*, 2010, **132**, 041303.

96 E. Aljallis, M. Sarshar, R. Datla, V. Sikka, A. Jones and C. Choi, *Phys. Fluids*, 2013, **25**, 025103.

97 N. Ivanova and V. Starov, *Curr. Opin. Colloid Interface Sci.*, 2011, **16**, 285–291.

98 Y. Nam, E. Aktinol, V. Dhir and Y. Ju, *Int. J. Heat Mass Transfer*, 2011, **54**, 1572–1577.

99 R. Waldman, H. Yang, D. Mandia, P. Nealey, J. Elam and S. Darling, *Adv. Mater. Interfaces*, 2018, **10**, 1800658.

100 C. Shan, J. Yong, Q. Yang, F. Chen, J. Huo, J. Zhuang, Z. Jiang and X. Hou, *AIP Adv.*, 2018, **8**, 045001.

101 R. Pugh, *Adv. Colloid Interface Sci.*, 1996, **64**, 67–142.

102 C. Yu, M. Cao, Z. Dong, J. Wang, K. Li and L. Jiang, *Adv. Funct. Mater.*, 2016, **26**, 3236–3243.

103 R. Ma, J. Wang, Z. Yang, M. Liu, J. Zhang and L. Jiang, *Adv. Mater.*, 2015, **27**, 2384–2389.

104 J. Yang, J. Duan, D. Fornasiero and J. Ralston, *Phys. Chem. Chem. Phys.*, 2007, **9**, 6327–6332.

105 I. Vakarelski, N. Patankar, J. Marston, D. Chan and S. Thoroddsen, *Nature*, 2012, **489**, 274.

106 B. Emami, H. Vahedi Tafreshi, M. Gad-el-Hak and G. Tepper, *Appl. Phys. Lett.*, 2012, **100**, 013104.

107 M. Chen, Z. Jia, T. Zhang and Y. Fei, *Soft Matter*, 2018, **14**, 7462–7468.

108 X. Yan, Y. Jia, L. Wang and Y. Cao, *Chem. Eng. J.*, 2017, **316**, 553–562.

109 L. Schiller and A. Nauman, *Z. Ver. Deutsch. Ing.*, 1935, **77**, 318–320.

110 J. Chen, Y. Liu, D. Guo, M. Cao and L. Jiang, *Chem. Commun.*, 2015, **51**, 11872–11875.

111 C. Pei, Y. Peng, Y. Zhang, D. Tian, K. Liu and L. Jiang, *ACS Nano*, 2018, **12**, 5489–5494.

112 H. Zhu, Z. Guo and W. Liu, *Chem. Commun.*, 2016, **52**, 3863–3879.

113 T. Xu, Y. Lin, M. Zhang, W. Shi and Y. Zheng, *ACS Nano*, 2016, **10**, 10681–10688.

This journal is © The Royal Society of Chemistry 2019

J. Mater. Chem. A, 2019, **7**, 12921–12950 | **12949**

114 O. Klemm, R. Schemenauer, A. Lummerich, P. Cereceda, V. Marzol, D. Corell, J. Van Heerden, D. Reinhard, T. Gherezghiher, J. Olivier, P. Osses, J. Sarsour, E. Frost, M. Estrela, J. Valiente and G. Fessehaye, *Ambio*, 2012, **41**, 221–234.

115 K. Park, P. Kim, A. Grinthal, N. He, D. Fox, J. Weaver and J. Aizenberg, *Nature*, 2016, **531**, 78.

116 M. Cao, J. Xiao, C. Yu, K. Li and L. Jiang, *Small*, 2015, **11**, 4379–4384.

117 F. Ren, G. Li, Z. Zhang, X. Zhang, H. Fan, C. Zhou, Y. Wang, Y. Zhang, C. Wang, K. Mu, Y. Su and D. Wu, *J. Mater. Chem. A*, 2017, **5**, 18403–18408.

118 R. Schemenauer and P. Cereceda, *J. Appl. Meteorol.*, 1994, **33**, 1313–1322.

119 R. Holmes, J. de Dios Rivera and E. de la Jara, *Atmos. Res.*, 2015, **151**, 236–249.

120 E. Shaulsky, S. Nejati, C. Boo, F. Perreault, C. Osuji and M. Elimelech, *J. Membr. Sci.*, 2017, **530**, 158–165.

121 K. Yin, H. Du, X. Dong, C. Wang, J. Duan and J. He, *Nanoscale*, 2017, **9**, 14620–14626.

122 H. Zhou, M. Zhang, C. Li, C. Gao and Y. Zheng, *Small*, 2018, **14**, 1801335.

123 L. Zhong, J. Feng and Z. Guo, *J. Mater. Chem. A*, 2019, **7**, 8405–8413.

124 L. Hu, S. Gao, Y. Zhu, F. Zhang, L. Jiang and J. Jin, *J. Mater. Chem. A*, 2015, **3**, 23477–23482.

125 Z. Wang, G. Liu and S. Huang, *Angew. Chem., Int. Ed.*, 2016, **55**, 14610–14613.

126 X. Yang, Z. Wang and L. Shao, *J. Membr. Sci.*, 2018, **549**, 67–74.

127 Z. Wang, Y. Wang and G. Liu, *Angew. Chem., Int. Ed.*, 2016, **55**, 1291–1294.

128 Y. An, J. Yang, H. Yang, M. Wu and Z. Xu, *ACS Appl. Mater. Interfaces*, 2018, **10**, 9832–9840.

129 X. Tian, H. Jin, J. Sainio, R. Ras and O. Ikkala, *Adv. Funct. Mater.*, 2014, **24**, 6023–6028.

130 J. Zuo, T. Chung, G. O'Brien and W. Kosar, *J. Membr. Sci.*, 2017, **523**, 103–110.

131 H. Yang, W. Zhong, J. Hou, V. Chen and Z. Xu, *J. Membr. Sci.*, 2017, **523**, 1–7.

132 A. Alkhudhiri, N. Darwish and N. Hilal, *Desalination*, 2012, **287**, 2–18.

133 Z. Wang and S. Lin, *Water Res.*, 2017, **112**, 38–47.

134 L. Tijing, Y. Woo, J. Choi, S. Lee, S. Kim and H. Shon, *J. Membr. Sci.*, 2015, **475**, 215–244.

135 Y. Huang, Z. Wang, J. Jin and S. Lin, *Environ. Sci. Technol.*, 2017, **51**, 13304–13310.

136 Y. Liu, T. Xiao, C. Bao, Y. Fu and X. Yang, *J. Membr. Sci.*, 2018, **563**, 298–308.

137 M. Qtaishat, M. Khayet and T. Matsuura, *J. Membr. Sci.*, 2009, **329**, 193–200.

138 M. Khayet, J. Mengual and T. Matsuura, *J. Membr. Sci.*, 2005, **252**, 101–113.

139 P. Tian, X. Gao, G. Wen, L. Zhong, Z. Wang and Z. Guo, *J. Colloid Interface Sci.*, 2018, **532**, 517–526.

140 W. Zhang, L. Wang, K. Sun, T. Luo, Z. Yu and K. Pan, *Sens. Actuators, B*, 2018, **268**, 421–429.

141 H. Cheng, F. Zhao, J. Xue, G. Shi, L. Jiang and L. Qu, *ACS Nano*, 2016, **10**, 9529–9535.

142 J. Yang, J. Zhang, X. Li, J. Zhou, Y. Li, Z. Wang, J. Cheng, Q. Guan and B. Wang, *Nano Energy*, 2018, **53**, 916–925.

143 J. Gylys, T. Zdankus and M. Gylys, *Int. J. Heat Mass Transfer*, 2014, **69**, 230–236.

144 M. Sarkar, S. Donne and G. Evans, *Adv. Powder Technol.*, 2010, **21**, 412–418.

145 M. Kermani and A. Morshed, *Corrosion*, 2003, **59**, 659–683.

146 A. Samimi, *International Journal of Science and Investigations*, France, 2012.

147 Y. Li, H. Zhang, T. Xu, Z. Lu, X. Wu, P. Wan, X. Sun and L. Jiang, *Adv. Funct. Mater.*, 2015, **25**, 1737–1744.

148 Z. Lu, Y. Li, X. Lei, J. Liu and X. Sun, *Mater. Horiz.*, 2015, **2**, 294–298.

149 J. Hou, M. Zulkifli, M. Mohamma, Y. Zhang, A. Razmjou and V. Chen, *J. Membr. Sci.*, 2016, **520**, 303–313.

150 H. Yang, J. Hou, L. Wan, V. Chen and Z. Xu, *Adv. Mater. Interfaces*, 2016, **3**, 1500774.

151 J. Hou, C. Ji, G. Dong, B. Xiao, Y. Ye and V. Chen, *J. Mater. Chem. A*, 2015, **3**, 17032–17041.

152 S. Gao, M. Mohammad, H. Yang, J. Xu, K. Liang, J. Hou and V. Chen, *ACS Appl. Mater. Interfaces*, 2017, **9**, 42806–42815.

153 S. Yan, F. Ren, C. Li, Y. Jiao, C. Wang, S. Wu, S. Wei, Y. Hu, J. Li, Y. Xiao, Y. Su and D. Wu, *Appl. Phys. Lett.*, 2018, **113**, 261602.

154 J. Jesty, M. Wieland and J. Niemiec, *J. Biomed. Mater. Res., Part B*, 2009, **89**, 536–542.

155 T. Zhu, J. Wu, N. Zhao, C. Cai, Z. Qian, F. Si, H. Luo, J. Guo, X. Lai and L. Shao, *Adv. Healthcare Mater.*, 2018, 7, 1701086.

156 Z. Tang, J. Lee, R. Louie and G. Kost, *Arch. Pathol. Lab. Med.*, 2000, **124**, 1135–1140.

157 W. Zhang, L. Hu, H. Chen, S. Gao, X. Zhang and J. Jin, *J. Mater. Chem. B*, 2017, **5**, 4876–4882.

12950 | *J. Mater. Chem. A*, 2019, **7**, 12921–12950

This journal is © The Royal Society of Chemistry 2019